Journal of Biomolecular NMR, 7 (1996) 8–28
ESCOM

J-Bio NMR 326

Comparison of the structure of human recombinant short form stromelysin by multidimensional heteronuclear NMR and X-ray crystallography*

Paul R. Gooley[a,**], John F. O'Connell[a], Alice I. Marcy[b], Gregory C. Cuca[a], Melinda G. Axel[a], Charles G. Caldwell[c], William K. Hagmann[c] and Joseph W. Becker[a]

Departments of [a]Biochemistry, [b]Molecular Design and Diversity and [c]Medicinal Chemical Research, Merck Research Laboratories, P.O. Box 2000, Rahway, NJ 07065, U.S.A.

Received 14 September 1995
Accepted 27 November 1995

Keywords: Stromelysin-1; MMP-3; Metalloprotease; Protein structure

Summary

Stromelysin-1 is a matrix metalloprotease that has been implicated in a number of degenerative diseases. Here we present the refined NMR solution structure of the catalytic domain of stromelysin-1 complexed with a small inhibitor and compare it to the X-ray crystal structure of the same complex. The structures are similar in global fold and show an unusual bottomless S1' subsite. There are differences, however, in the least well defined regions, Phe^{83}–Ile^{89}, His^{224}–Phe^{232} and Pro^{249}–Pro^{250}, reflecting the lack of NOE data and large B-factors. The region His^{224}–Phe^{232} contains residues of the S1' subsite and, consequently, small differences are observed in this subsite. Hydrogen-bond data show that, in contrast to the crystal structure, the solution structure lacks a hydrogen bond between the amide of Tyr^{223} and the carbonyl of the P3' residue. Analysis of bound water shows two tightly bound water molecules both in the solution and the crystal structure; neither of these waters are in the inhibitor binding site.

Introduction

Stromelysin-1 (MMP-3) belongs to the matrix metalloprotease (MMP) family, which includes the collagenases, gelatinases, stromelysins and matrilysins (Woessner, 1991). These enzymes are zinc and calcium dependent and their normal physiological function is the degradation of the extracellular matrix. They have been implicated in a number of diseases, including osteo- and rheumatoid arthritis (Dean et al., 1989; Hasty et al., 1990; McCachren et al., 1990), corneal ulceration (Brown et al., 1969), periodontal disease (Overall et al., 1987), and degradation of the basement membrane in cancer metastasis (Matrisian et al., 1986). While the activity of these proteinases is controlled in vivo by endogenous inhibitors such as α-macroglobulin and tissue inhibitor of metalloendoproteases (TIMP-1 and -2), the disease state may be a consequence of an imbalance in the ratio of protease to protease inhibitor. Several observations suggest that stromelysin-1 plays a significant role in pathological proteolysis of connective tissue: the enzyme has a broad substrate specificity (Welgus, 1991; Wu et al., 1991), both messenger and protein levels are elevated in pathological states (Gravallese et al., 1991; Okada et al., 1992) and stromelysin-1 appears to activate other MMPs (Murphy et al., 1987; Ito and Nagase, 1988). In the disease state, a potent synthetic inhibitor of stromelysin-1 may have therapeutic effects by restoring the ratio of protease to protease inhibitor to physiological levels.

An initial NMR solution structure of the catalytic domain of inhibited stromelysin-1 (sfSTR) has been determined (Gooley et al., 1994). The crystal structures of the same inhibited complex and of prostromelysin-1 (Becker

*The coordinates of the NMR solution structure (file name 2SRT) and the X-ray crystal structure (file name 1SLN) have been deposited in the Brookhaven Protein Data Bank.

**To whom correspondence should be addressed at: Department of Biochemistry, University of Melbourne, Parkville, Victoria 3052, Australia.

Abbreviations: MMP, matrix metalloendoprotease; HMQC, heteronuclear multiple quantum coherence; HSQC, heteronuclear single quantum coherence; NOE, nuclear Overhauser enhancement; NOESY, NOE spectroscopy; PFG, pulsed field gradient; sfSTR, stromelysin-1 (EC 3.4.24.17), truncated at residue 255.

et al., 1995) and two other MMPs have been determined, i.e., fibroblast (Borkatoti et al., 1994; Lovejoy et al., 1994; Spurlino et al., 1994) and neutrophil collagenase (Bode et al., 1994; Stams et al., 1994; Grams et al., 1995), as well as those of other related metalloproteases, the digestive enzyme astacin from crayfish (Bode et al., 1992; Gomis-Rüth et al., 1993b) and the snake venom metalloproteases adamalysin II (Gomis-Rüth et al., 1993a) and atrolysin C (Zhang et al., 1994) and a serralysin from *Serratia marcescens* (Baumann, 1994). In all these proteases the ligation of the catalytic zinc ion involves the three histidine residues of the consensus sequence, HEXXHXXGXXH, while in the astacin family tyrosine appears to be a fourth ligand. These enzymes have similar regular secondary structural elements, i.e., a five-stranded β-sheet and three helices. An additional common structural feature of these enzymes is a methionine residue (Met^{219} in sfSTR) located in a turn near the catalytic histidine residues. These topological similarities of an α/β core, a methionine turn and an HEXXHXXGXXH zinc-binding domain have suggested that these zinc endoproteases, including the astacin family (Dumermuth et al., 1991), the bacterial zinc endoproteases (Häse and Finkelstein, 1994), the adamalysins (Fox et al., 1986), and the MMP family (Murphy et al., 1991), belong to a new protein class, the metzincins (Bode et al., 1993; Stöcker et al., 1995). The distinguishing feature of sfSTR and other members of the MMP family is the additional structural zinc ligated by three histidines and an aspartic acid (Salowe et al., 1992; Gooley et al., 1993; Lovejoy et al., 1994). The histidine residues that ligate the structural zinc are invariant amongst the MMP members, but absent in the astacin family. The loop in sfSTR that joins strands III and IV (Gooley et al., 1994) and contains the zinc ligands His^{151} and Asp^{153} is 15 residues long, compared to three residues in astacin, suggesting that zinc ligation stabilizes this longer loop in the MMPs. The MMPs also contain one to three calcium ions, consistent with the requirement of this metal for activity.

In this paper we present the refined solution structure of sfSTR complexed with a small *N*-carboxyalkyl inhibitor (Chapman et al., 1993). The details of this structure are discussed and compared to the X-ray crystal structure of the same complex, which has been solved independently in our laboratories (Becker et al., 1995). Comparisons are made with respect to the secondary structure, the global fold, the (ϕ,ψ) plots, potential hydrogen bonds, the presence of bound water, and intermolecular contacts.

Methods

NMR spectroscopy

NMR data were collected on Varian 500 MHz Unity, 600 MHz Unity or 600 MHz Unity plus systems with triple resonance or PFG triple resonance probes. Protein purification, sample preparation, spectra acquired for resonance assignments, and their analysis have been described elsewhere (Marcy et al., 1991; Gooley et al., 1993). The sample conditions were typically 0.6 mM protein in 50 mM $CD_3COO^-Na^+$, 5 mM $CaCl_2$, 0.02% NaN_3, pH 5.5 at 40 °C. After the samples were prepared, they contained approximately 10% excess of the inhibitor *N* [1(*R*)-carboxyethyl]-α-(*S*)-(2-phenylethyl)glycine-L-arginine-*N*-phenylamide (Chapman et al., 1993). Additional spectra acquired were ^{13}C and ^{15}N NOESY spectra (50 and 100 ms mixing time) (Zuiderweg and Fesik, 1989; Ikura et al., 1990), 3D ^{13}C-separated/^{13}C-filtered NOESY (Gooley et al., 1994), and 2D ^{15}N-filtered and $^{13}C/^{15}N$ time-shared-filtered NOESY (Burgering et al., 1993), all recorded with mixing times of 100 ms. Other spectra acquired to confirm assignments and to provide quantitative and qualitative coupling constant information were 3D HNHa ($^3J_{HNH\alpha}$) (Vuister and Bax, 1993), 3D HNHb ($^3J_{NH\beta}$) (Archer et al., 1991) and 3D HCaCO ($^1J_{C'C\alpha}$) (Powers et al., 1991; Vuister et al., 1992). Spectra were processed with either FELIX (Biosym, Inc., San Diego, CA) or NMRPipe (Delaglio et al., 1995) and analyzed with NMRView (Johnson and Blevins, 1994).

NH exchange

To support hydrogen-bond analysis, exchange rates of NH protons with solvent protons were determined. Experiments were performed with a sample of an inhibitor where the P2' residue was leucine instead of arginine, and the P2' and P3' residues were labeled with ^{15}N. Firstly, a sample was prepared in buffer with 100% H_2O, then this solution was exchanged three times with buffer prepared with 100% D_2O at 4 °C (preparation time 45 min). The sample was placed in the spectrometer at 40 °C for 10 min and a 2D $^1H,^{15}N$ HSQC spectrum was acquired in 45 min. Protons assigned to NH resonances that persist in this spectrum were considered to have exchange rates $\ll 1$ s^{-1}. Secondly, a series of experiments were performed to determine the rates of fast exchanging NH protons, as follows. 2D saturation transfer-difference $^1H,^{15}N$ HSQC spectra were acquired at pH 5.5, 6.5 and 7.5 (Spera et al., 1991). It was necessary to record these experiments at different pH values to determine the effect of saturating COOH, OH, NH_3^+ and $C^\alpha H$ protons, which resonate at the water frequency, on attenuating signals of NH protons nearer than 4 Å. These effects are largely pH independent, whereas exchange with the protons of water is pH dependent. The spectra were acquired with 16 scans of weak water saturation (30 Hz) and 16 scans without saturation. The pulse sequence included flip-back pulses and a WATERGATE sequence to suppress the water signal (Grzesiek and Bax, 1993a). The exchange rates (k_{hx} (s^{-1})) were determined using the equations of Spera et al. (1991). Spin-relaxation times (T_1) for 30 slowly exchanging NH protons were determined by recording a series of

2D experiments as previously described (Wagner et al., 1993). The average T_1 was 90.9±19.3 ms; the values ranged from 63.8 to 131.3 ms.

Localization of water

To determine the presence of tightly bound water, 2D water-ROE and water-NOE PFG-$^1H,^{15}N$ and $^1H,^{13}C$ HSQC spectra were acquired (Grzesiek and Bax, 1993b) with the water alternately aligned along the +z- and –z-axis. To invert the water selectively, weak π and π/2 SEDUCE pulses (60 and 30 Hz field strength, respectively) were used (McCoy and Mueller, 1992). To remove signals from ^{13}C-attached protons, two purge pulses were applied (Clore et al., 1994). Either a 25 ms, 10 kHz spin-lock (ROE) or a 60 to 80 ms mixing time (NOE) was used and the detection period was a $^1H,^{15}N$ or $^1H,^{13}C$ HSQC, using flip-back pulses and a WATERGATE sequence (Grzesiek and Bax, 1993a). Control experiments identical to the 2D water-NOE experiments were performed, where the selective pulses for water were preceded by 0.8 s of presaturation (10 Hz), followed by a delay of 0.2 s (Clore et al., 1994). All unambiguous peaks were assigned in the spectra. Protons that showed NOEs and ROEs to water were examined in the structure of sfSTR to see if they were near groups that are in rapid exchange with water: OH (threonine, serine, tyrosine), NH_3^+ (lysine), guanidinium NH (arginine) and COOH (aspartic acid, glutamic acid). An NH proton was considered to be near one of these groups if the average distance was less than 5 Å between the proton and the heavy atom (oxygen or nitrogen) of the exchanging group in the 30 solution conformers and/or the crystal structure. Similarly, methyl groups were examined where the average cutoff distance was 6 Å between the heavy atoms of the methyl and the exchangeable group. The carboxylates of Asp[153] and Asp[158] were excluded, as these groups ligate zinc and calcium, respectively, and therefore are deprotonated. Thr[98] and Tyr[246] were excluded as well, as the hydroxyl protons of these residues resonate at 5.24 and 10.24 ppm, respectively, and are therefore not affected by the selective inversion pulse. These hydroxyl protons were observed in ^{15}N-filtered NOESY spectra and were consistent with being attached to oxygen, as they were absent in ^{13}C spectra. Their intraresidue NOE patterns were also consistent with their assignment.

Structure calculations

NOE intensities were converted to distances using CALIBA, v. 2.1 (Güntert et al., 1991), where NOEs between NH, $C^\alpha H$ and $C^\beta H$ atoms were calibrated assuming the NOE intensity to be proportional to r^{-6} and all other NOEs were calibrated assuming the NOE intensity to be proportional to r^{-4} (Suri and Levy, 1993), thus allowing for side-chain flexibility. Calibration of the NOEs in ^{15}N NOESY spectra to distances was accomplished by using the known sequential distances NH-H^α and NH-NH in β-strands and helices, respectively, as a guide. The constraints were tightened periodically throughout the iterative assignment–calculation process until the majority of these distances were well satisfied. The calibration of the ^{13}C NOESY spectra was more difficult, as there are fewer known distances to calibrate against. The distance between the $C^\alpha H$ and $C^\delta H$ of a trans X-Pro peptide bond is 2.2–3.9 Å. The final calibration of the ^{13}C NOESY spectra showed that the 11 proline residues of sfSTR that are in a defined structure were within these distances. In addition, the distance $C^\alpha H$-$C^\alpha H$ in an antiparallel β-sheet is approximately 2.3 Å and thus is a useful guide. There are three pairs of $C^\alpha H$-$C^\alpha H$, i.e., Ala[165] to Phe[180], Ala[167] to Ala[178] and Val[163] to the P2' arginine of the inhibitor. Our final calibration used the distances 3.3, 2.9 and 2.8 Å, respectively. These distances are at least 0.5 Å longer than expected, indicating that the data are not overcalibrated. The final distances for these three $C^\alpha H$-$C^\alpha H$ pairs in the final 30 structures are 2.5±0.22, 2.6±0.11 and 2.2±0.1 Å, respectively, which is in good agreement with the model distances.

Dihedral angle constraints were derived from HABAS, v. 2.1 (Güntert et al., 1989), modified for heteronuclear couplings ($^3J_{NH\beta}$), using the intraresidue and sequential NOEs. These data were complemented with 82 measured $^3J_{HNH\alpha}$ couplings from 3D HNHa and 44 approximate $^3J_{NH\beta}$ couplings from 3D HNHb spectra (Archer et al., 1991; Vuister and Bax, 1993). In the 3D HNHa spectrum an additional 27 $^3J_{HNH\alpha}$ couplings were estimated for two situations: firstly, where the cross peak was too weak but a resolved diagonal peak was observed (14 $^3J_{HNH\alpha}$), an expected maximum coupling could be estimated by using the intensity of the weakest peak in the spectrum, and secondly, where the cross peak was intense but the diagonal peaks either overlapped (nine $^3J_{HNH\alpha}$) or were too weak (four $^3J_{HNH\alpha}$), the coupling was estimated using the diagonal intensity of residues in similar structural elements or assuming the intensity of the weakest peak, respectively. The former situation was common for helical elements and the latter for β-sheets. The assumed error for all couplings was ±2 Hz. In addition, 120 $^1J_{C'C\alpha}$, measured in coupled 3D HCaCO spectra (Vuister et al., 1992), were greater than 140 Hz and thus the respective φ angle was restricted to the range –5 to –175°. For Arg[149] and Asn[162] the measured $^1J_{C'C\alpha}$ were 131 and 138 Hz, respectively, suggesting that their φ angles could be confined to the range +5 to +175°. However, we chose a conservative approach and did not include these two angles in the experimental constraints.

Structures were calculated with DIANA, v. 2.1 (Güntert et al., 1991) and energy minimized with FANTOM, v. 3.2 (Schaumann et al., 1990) on either a four-processor CRAY Y-MP/i4128 or a cluster of five IBM RS6000/580 computers. To improve convergence, four rounds of

REDAC (Güntert and Wüthrich, 1991) were applied. In the first three rounds 50 structures were calculated; after each round a new set of angle constraints were derived. In the final round 80 structures were calculated. These structures were recalculated at the final level (all residues) with the original dihedral angle constraints. From this calculation 30 structures were selected for minimization with FANTOM by plotting the target function against the maximum pairwise rmsd and selecting the first major plateau, where rmsd and target function are independent (Widmer et al., 1993). The plateau occurred between structures 26 and 56. Of these structures the first 26 were selected and an additional 4 from the remaining 30 (including the 56th). The barrier energy for the Ω angle in FANTOM was increased 10-fold to maintain planarity of the peptide bond.

The inhibitor residue template was constructed in X-PLOR, v. 3.1 (Brünger, 1992) and converted to the DIANA and FANTOM formats. The template consists of the inhibitor, a zinc atom and a histidine (His^{201} was always used). The residue is constructed such that an oxygen of the carboxylate of the inhibitor is attached to a zinc that is attached to the N^{ε} of the histidine. The distances and bond angles for the N^{ε}-Zn-O moiety and the appropriate impropers were derived from ab initio calculations (J.F. O'Connell, unpublished results). A second template was similarly constructed with a histidine (His^{151}) bonded to a zinc, assuming a distance of 2.03 Å (Gooley et al., 1994).

X-ray structure

The crystal structure of the complex between sfSTR and *N*[1(*R*)-carboxyethyl]-α-(*S*)-(2-phenylethyl)glycine-L-arginine-*N*-phenylamide was solved at a nominal resolution of 2.26 Å (Becker et al., 1995). Crystals were grown by vapor diffusion of a solution containing 9 mg/ml sfSTR, 1.5 mM inhibitor, 5.0 mM $CaCl_2$, 0.02% NaN_3, 20 mM Tris-HCl, pH 7.5, versus a reservoir containing 10% PEG-6000, 15% saturated NH_4OAc, 0.02% NaN_3, 0.1 M cacodylate, pH 5.54. The crystal structure of the inhibited complex comprises residues 83–250, two Zn^{2+} ions, three Ca^{2+} ions, the bound inhibitor, and 51 ordered water molecules. The refined model has a crystallographic R-factor of 22.3% (R_{free} = 29.8%) and rms deviations from ideal values (Engh and Huber, 1991) of 0.009 Å in bond lengths and 1.44° in bond angles.

Hydrogen atom positions for the X-ray structure were calculated in X-PLOR using only stereochemical criteria. Before crystallographic refinement, heavy atom positions were fixed and hydrogen atom positions were refined using only the electrostatic and van der Waals energy functions. The resulting coordinate set was used to initiate crystallographic refinement. Only heavy atoms contributed to the diffraction term in X-PLOR refinements.

Structure analysis and comparison to X-ray crystal structure

Experimental violations, potential hydrogen bonds, intermolecular contacts, rmsd values and solvent accessibility were determined by modifying the program XAM (Xia, 1992). The analysis of consistent NOE and experimental dihedral angle violations used cutoffs of 0.3 Å and 5°, respectively. Potential hydrogen bonds were evaluated by calculating the electrostatic interaction energy between the hydrogen-bonding atoms with the formula (Kabsch and Sander, 1983):

$$E = q_1 q_2 (1/r_{ON} + 1/r_{CH} - 1/r_{OH} - 1/r_{CN}) f \qquad (1)$$

where $q_1 = 0.42e$ and $q_2 = 0.20e$ (e being the unit electron charge), r_{AB} (in Å) is the interatomic distance from nucleus A to B, the dimensional factor f = 332, and E is in kcal/mol. An ideal hydrogen bond is −3 kcal/mol, and thus a cutoff of −1 kcal/mol was used for both structures. Intermolecular contacts between the protein and the inhibitor for the crystal and solution structures were assessed with cutoff distances of 4.0 Å and 4.5 ± 0.5 Å between heavy atoms, respectively (Spitzfaden et al., 1994). Solvent accessibility was determined using a probe of 1.4 Å. The φ,ψ angles and Kabsch–Sander secondary structure were calculated using XAM or PROCHECK (Morris et al., 1992).

Results and Discussion

Assignment of resonances and NOEs

Assignments of the ^1H, ^{13}C and ^{15}N spectra of inhibited sfSTR and the protons of the unlabeled inhibitor have been previously described (Gooley et al., 1993,1994). The extension and correction of these assignments have been completed through further analysis of the 3D heteronuclear NOESY and J-correlated spectra, including 3D HNHb and HNHa. The complete assignments can be obtained from the corresponding author as supplementary material. Assignment of many of the missing resonances required near-complete assignment of the 3D ^{13}C NOESY spectra. Using the expected chemical shift of the side-chain ^{13}C resonances, several residues that did not show scalar couplings could be assigned in these spectra: Phe^{83}, Arg^{100}, Asp^{158}, Glu^{184}, Glu^{202}, Met^{143} and Met^{219}. Two major corrections to the published assignments (Gooley et al., 1993) are that the assignment of the side chains of Leu^{218} and Leu^{226} are swapped and the chemical shifts of Phe^{83} are reassigned to Phe^{210}. The reassignment of the leucine side chains was realized after comparison of the initial solution structure of inhibited sfSTR with that of the crystal structure of a different form of inhibited sfSTR (J.W. Becker, unpublished results). The initial assignment of the spin system to Phe^{83} was based on NOEs to Arg^{84}. An additional phenylalanine system, which

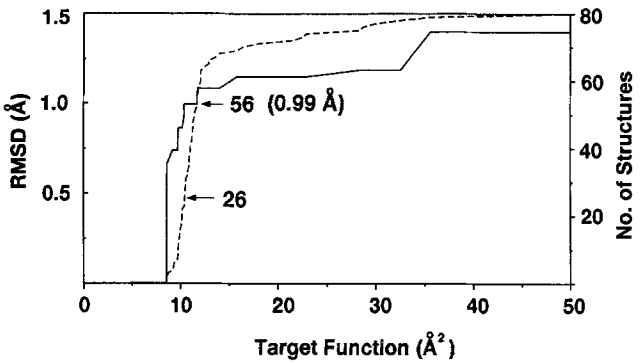

Fig. 1. Plot of maximum pairwise rmsd values (solid line) and number of calculated structures (dashed line) versus target function. At the plateau of 0.99 Å, 30 structures were selected: the first 26 structures and four structures between structures 26 and 56, including structure 56 itself.

shows NOEs to Thr^{85} and to Asn^{240}, was subsequently assigned. These NOEs are consistent with an interaction of the N-terminus of sfSTR with residues near Asn^{240}, as observed in the crystal structure of collagenase (Bode et al., 1994), thus supporting the reassignment of Phe^{83} and Phe^{210}.

The methyl groups of leucine and valine residues were stereospecifically assigned in 10% $^{1}H,^{13}C$ HMQC spectra, where the $C^{\delta 2}H_3$ and $C^{\gamma 2}H_3$, respectively, appear as singlets (Neri et al., 1989). β-Methylene groups were stereospecifically assigned by considering intraresidue NOEs from ^{13}C and ^{15}N NOESY spectra ($\tau_m = 50$ ms), sequential NOEs from ^{15}N NOESY spectra ($\tau_m = 50$ and 100 ms), and assignment of β-protons in a 3D HNHb spectrum. Of the 93 residues that showed two nondegenerate β-protons, 51 were stereospecifically assigned. The remainder either showed equivalent NOEs in the NOESY spectra, indicating rotamer averaging, or the data were insufficiently clear for stereoassignment. Only 16 pairs of β-protons were unambiguously stereoassigned using HABAS. The remainder were considered ambiguous by this program; however, comparison of the peak intensities in the NOESY spectra (NH-$C^{\beta 1}H$ compared to NH-$C^{\beta 2}H$ and $C^{\alpha}H$-$C^{\beta 1}H$ compared to $C^{\alpha}H$-$C^{\beta 2}H$) and the presence or absence of peaks in 3D HNHb spectra guided the stereospecific assignment of the β-protons of the other 37 residues.

Structure calculation and selection

The initial structures calculated for inhibited sfSTR (Gooley et al., 1994) were used to further assign the NOE spectra. NOEs involving NH protons were derived from 3D ^{15}N NOESY spectra with mixing times of 50 and 100 ms; interresidual NOEs involving only ^{13}CH protons were from 3D and 4D ^{13}C NOESY spectra ($\tau_m = 100$ ms) and the intraresidue NOEs of ^{13}CH protons from a 3D ^{13}C NOESY ($\tau_m = 50$ ms); NOEs between ^{13}C-attached protons of the protein and ^{12}C-attached protons of the inhibitor were assigned in a 3D ^{13}C-separated, ^{13}C-filtered NOESY and these assignments were extended in 3D ^{13}C NOESY spectra; NOEs from the ^{14}N-attached protons of the inhibitor to protons of the protein were assigned in 2D ^{15}N-filtered NOESY spectra; and NOEs between the protons of the inhibitor were assigned in 2D ^{13}C-filtered, 2D ^{15}N-filtered and 2D ^{13}C-/^{15}N-filtered NOESY spectra. To generate further assignments of ambiguous NOEs, an iterative process of assignment and calculation was exploited. The final number of unique assigned peaks in the NOE spectra was 2589. After treatment with DIANA, fixed distance, nonconstraining and ambiguous intraresidue NOEs were removed, leaving 1814 meaningful distance constraints: 325 intraresidue, 429 sequential, 324 short range ($i+2$ to $i+5$), 665 long range ($>i+5$) and 71 intermolecular. Using the program HABAS, 379 dihedral angles (140 ϕ, 140 ψ and 99 χ^1) were generated from the sequential and intraresidue NOE and coupling constant data. Potential hydrogen bonds of the sheet and helices were used to aid the fold and convergence of the structure calculation; however, after assignment of approximately 1200 distance constraints these hydrogen bonds were no longer used. To reduce biases in structure selection, plots of the rmsd and number of structures versus target function of the final 80 structures were used to select structures for FANTOM minimization (Fig. 1) (Widmer et al., 1993). In the final calculations, 30 structures were selected. Table 1 summarizes the DIANA and FANTOM statistics for these 30 structures.

The structure of sfSTR

Figure 2 shows a ribbon diagram of the lowest energy conformer of inhibited sfSTR. The global fold of sfSTR has been described (Gooley et al., 1994) and is identical

TABLE 1
STRUCTURAL STATISTICS OF THE 30 CONFORMERS REPRESENTING THE SOLUTION STRUCTURE OF sfSTR COMPLEXED WITH *N*[1(*R*)-CARBOXYETHYL]-α-(*S*)-(2-PHENYLETHYL)GLYCINE-L-ARGININE-*N*-PHENYLAMIDE

Parameter	DIANA	FANTOM
DIANA target function (Å²)	10.01 ± 0.76	
FANTOM energy (kcal/mol)		−191.0 ± 52.8
Lennard-Jones energy (kcal/mol)		−605.4 ± 48.4
Distance constraint violations (Å)		
Sum	35.2 ± 1.2	61.6 ± 1.4
Maximum	0.48 ± 0.06	0.39 ± 0.03
Rmsd	0.06 ± 0.01	0.08 ± 0.01
Exp. angle constraint violations (°)		
Sum	93.4 ± 11.1	112.1 ± 19.9
Maximum	7.5 ± 0.9	12.6 ± 5.0
Rmsd	0.90 ± 0.08	1.2 ± 0.3
Rmsd residues 83–250 (Å)		
Backbone (C^{α},N,C',O)	0.48 ± 0.06	0.55 ± 0.06
All heavy atoms	0.94 ± 0.06	0.97 ± 0.05

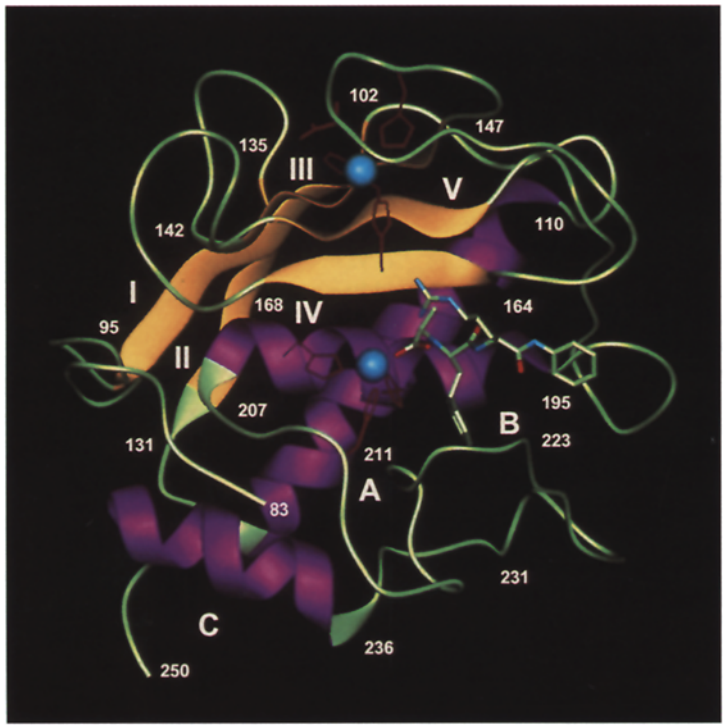

Fig. 2. Ribbon structure of the lowest energy conformer for the NMR solution structure of inhibited sfSTR, residues 83–250. The two zinc atoms are shown as large balls. The side-chain heavy atoms of the ligands of the two zincs are shown: for the catalytic zinc, these are His^{201}, His^{205}, His^{211} and the inhibitor and for the structural zinc, these are His^{151}, Asp^{153}, His^{166} and His^{179}. Helices are labeled A–C and the strands of the β-sheet are indicated by I–V.

to that of other metzincins, including astacin (Bode et al., 1992), adamalysin II (Gomis-Rüth et al., 1993a), and two MMPs, neutrophil (Bode et al., 1994; Stams et al., 1994; Grams et al., 1995) and fibroblast collagenase (Borkatoti et al., 1994; Lovejoy et al., 1994; Spurlino et al., 1994). The structure can be summarized as follows. sfSTR consists of a five-stranded β-sheet, comprising four parallel and one antiparallel strands with the topology –1x,+2x, +2,–1 (Richardson, 1977). The β-sheet lies on two helices (helices A and B), and a third helix (helix C) is near the carboxy terminus. The MMPs differ from the adamalysins and astacins in that they have a structural zinc ion in addition to the catalytic zinc. The two histidine residues in helix B, His^{201} and His^{205}, and a third histidine, His^{211}, ligate the catalytic zinc. The fourth ligand is an oxygen from the carboxylate of the inhibitor or, presum-

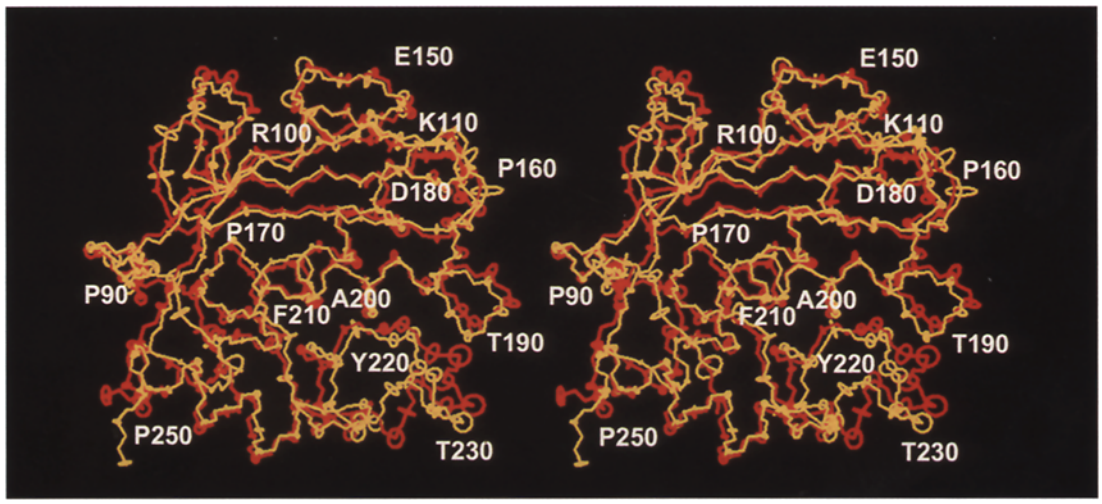

Fig. 3. Superposition of the heavy backbone atoms (C^{α}, N, O, C') of the crystal (red) and the average coordinates of the solution structure of inhibited sfSTR (yellow). The uncertainties of these coordinates are shown as circles and are derived from the B-factors for the crystal structure, $B = (8\pi^2/3)\Delta r_i^2$ where Δr_i^2 is the mean square atomic positional fluctuation, and the rmsd for the solution structure.

TABLE 2
VIOLATIONS OF EXPERIMENTAL NOE CONSTRAINTS IN THE CRYSTAL STRUCTURE[a]

Atoms assigned to NOE				NMR exp. distance (Å)	Measured distance (Å)	Difference (Å)
Ala^{116}	$H^{\beta\#}$	Ala^{199}	H^{α}	5.40	7.55	2.15
Lys^{119}	$H^{\epsilon\#}$	Leu^{229}	$H^{\delta2\#}$	5.98	9.62	3.64
Val^{127}	H^{α}	Pro^{248}	$H^{\gamma2}$	4.10	8.55	4.45
Val^{127}	H^{α}	Pro^{248}	$H^{\gamma1}$	4.10	7.89	3.79
Val^{127}	H^{α}	Pro^{248}	$H^{\delta\#}$	4.88	8.59	3.71
Val^{127}	$H^{\gamma2\#}$	Pro^{248}	$H^{\gamma\#}$	5.98	10.37	4.39
Thr^{128}	H^{α}	Pro^{248}	$H^{\gamma2}$	4.50	6.96	2.46
Pro^{129}	H^{α}	Pro^{248}	H^{α}	3.30	6.84	3.54
Pro^{129}	H^{α}	Pro^{248}	$H^{\gamma\#}$	5.18	8.23	3.05
Pro^{129}	H^{α}	Pro^{249}	$H^{\delta1}$	3.90	7.06	3.16
Pro^{129}	H^{α}	Pro^{249}	$H^{\delta\#}$	3.65	6.49	2.84
Pro^{129}	H^{α}	Pro^{249}	$H^{\delta2}$	3.90	5.99	2.09
Thr^{190}	$H^{\gamma2\#}$	Asp^{228}	H^{α}	5.00	7.09	2.09
Thr^{190}	$H^{\gamma2\#}$	Leu^{229}	H^{N}	4.70	7.26	2.56
Leu^{197}	$H^{\delta2\#}$	Ser^{225}	H^{α}	5.30	8.26	2.96
Leu^{197}	H^{γ}	INH	H^{η}	3.80	5.80	2.00
Leu^{197}	$H^{\delta1\#}$	INH	H^{η}	3.40	5.47	2.07
His^{205}	H^{α}	Phe^{210}	H^{ζ}	4.70	9.29	4.59
His^{205}	$H^{\beta1}$	Phe^{210}	H^{ζ}	4.70	8.84	4.14
Leu^{218}	$H^{\delta1\#}$	Leu^{234}	$H^{\delta1\#}$	6.40	8.52	2.12
Leu^{226}	$H^{\beta2}$	Phe^{232}	H^{α}	4.80	6.98	2.18
Leu^{229}	$H^{\delta1\#}$	Phe^{232}	$H^{\beta1}$	4.70	7.09	2.39
Leu^{229}	$H^{\delta1\#}$	Phe^{232}	C^{γ}	6.10	8.27	2.17

[a] Experimental distances were derived from NOE data. Some experimental distances have been adjusted to include pseudoatoms (# or heavy atom). Measured distances are for the crystal structure. Experimental distances that are violated by more than 2 Å are listed.

ably, water in mature uninhibited sfSTR. Similarly, three histidine residues ligate the structural zinc: two of these, His^{166} and His^{179}, are from opposing antiparallel β-strands and the third, His^{151}, is from a 15-residue loop that connects strands III and IV. The fourth ligand is an oxygen of the carboxylate of Asp^{153}, also from this loop. The inhibitor binding site is characterized by a cleft, to which the backbone of the inhibitor binds in an extended manner, and by a bottomless S1' subsite, which is discussed in detail below.

The family of structures has been analyzed with respect to ϕ,ψ angles, regular and nonregular structure, hydrogen bonds and intermolecular contacts and has been compared to the structure of the same complex determined by X-ray crystallography (Becker et al., 1995). These analyses and comparisons have revealed the following details.

Comparison of fold of the NMR solution and X-ray crystal structures

In Fig. 3 the crystal and average solution structures are superimposed. The rmsd of the heavy backbone atoms (C^{α}, C', O, N) for Phe^{83}–Pro^{250} of the protein, those of the inhibitor and the two zincs between these structures is 1.51 Å and for all heavy atoms it is 2.18 Å. The rmsd of the backbone atoms shows significant deviations for the regions Phe^{83}–Gly^{88}, His^{224}–Arg^{231} and Pro^{249}–Pro^{250}. If these regions are excluded (10% of the protein), the rmsd of the heavy backbone atoms is 1.21 Å and for all heavy atoms it is 1.94 Å. Two of these regions, Phe^{83}–Gly^{88} and His^{224}–Arg^{231}, appear to be functionally important and are discussed below. The third region, Pro^{249}–Pro^{250}, precedes the five remaining residues of the disordered C-terminal tail, which is not visible in the crystal structure and is

TABLE 3
VIOLATIONS OF EXPERIMENTAL ANGLE CONSTRAINTS IN THE CRYSTAL STRUCTURE[a]

Assigned angle		Range of experimental angle (°)	Measured angle (°)	Difference (°)
Glu^{126}	χ^1	135.0 – –115.0	–64.3	50.7
Glu^{137}	χ^1	35.0 – 85.0	–64.4	99.5
Glu^{150}	χ^1	145.0 – –145.0	–72.2	72.8
Tyr^{155}	χ^1	15.0 – 115.0	–69.2	84.2
Asp^{177}	χ^1	115.0 – –115.0	–56.3	58.7
Gln^{185}	ψ	155.0 – –165.0	99.7	55.3
Leu^{229}	χ^1	100.0 – 140.0	–95.8	124.2

[a] Experimental angles were derived from coupling constant data. Measured angles are for the crystal structure. Experimental angles that are violated by more than 50° are listed.

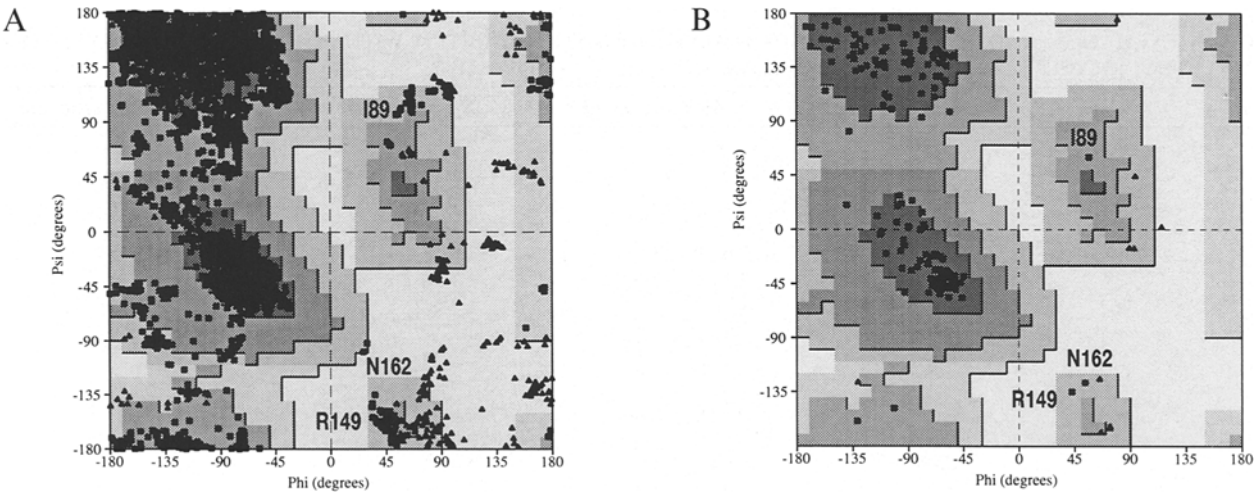

Fig. 4. Ramachandran plots for all 30 solution conformations of inhibited sfSTR (A) and the crystal structure (B) for residues 83–250. The last five residues are disordered and are not included in the plots. Triangles represent glycine residues.

characterized by only eight NOEs in the solution structure. This region does not appear to be either functionally or structurally significant, as fully active constructs extending only to residue 247 have been made (A.I. Marcy, R.T. Cummings and M.G. Axel, unpublished results; Ho et al., 1994).

The Ramachandran plot for residues 83–250 of the 30 solution conformers of the complex is shown in Fig. 4A, and the corresponding plot for the crystal structure in Fig. 4B. For the solution structure, 76% of the residues are within the most favored regions, compared to 88% for the crystal structure. For both the crystal and the family of solution structures, no nonglycine and nonproline residues are found in disallowed regions. In the crystal structure, Ile[89], Arg[149] and Asn[162] are located in the allowed regions in the right-hand part of the Ramachandran plot. These residues are consistently found in the same regions of the plot for the family of solution structures. The $^{1}J_{C'C\alpha}$ coupling measured for both Arg[149] and Asn[162] was less than 140 Hz, consistent with their ϕ angle. This coupling could not be measured for Ile[89].

The crystal structure was analyzed to assess the agreement between this structure and the experimental NMR restraints. Of the 1814 distance constraints, 150 are violated by more than 0.5 Å; 23 of these are violated by more than 2.0 Å (Table 2). Of the 381 angle constraints, 15 are violated by more than 50° (Table 3). Of these distance violations, 10 are between the C-terminal region, Pro[248]–Pro[249], and the C-terminal end of helix A, Thr[126] to Pro[129]. Other regions include Leu[197] and residue P1' of the inhibitor, and residues in the 220s with residues in the 230s. These differences are discussed below. Another violation is observed between His[205] and Phe[210]. From the crystal structure, it can be concluded that this violation may be due to an NOE misassignment that should be to Phe[86] and not Phe[210]. The H^{ζ} proton is within 5 Å of the H^{β} protons of His[205]. This error appears to affect only the local structure of Phe[210].

Regular secondary structure: β-sheet and helix

The five strands of the β-sheet encompass the following residues: strand I, the carbonyl of Thr[95] to the NH of Val[102]; strand II extends from the NH of Thr[131] to the amide of Leu[135]; strand III, from the NH of Ile[142] to the carbonyl of Ala[147]; strand IV, the carbonyl of Leu[164] to NH of Tyr[168]; and strand V, the carbonyl of Ala[178] to the NH of Asp[182]. The solution and crystal structures for the sheet are in good agreement. The hydrogen bonds of these strands are typical (Table 4); however, several additional interactions are noted. In both structures the ends of strand III are further stabilized by several interactions between NH protons and side-chain groups, i.e., between the NH of Asp[141] and the $O^{\gamma 1}$ of Thr[98] as well as the NH of Phe[146] and the $O^{\gamma 1}$ of Asn[103]. An additional interaction observed in the crystal structure is a hydrogen bond between the NH of Met[143] and the COO^{-} of Asp[177]. This hydrogen bond is not predicted in the solution structure, where the nitrogen is 4.5 ± 0.6 Å from the oxygens of the carboxylate of Asp[177]. Notably, the NH of Met[143] does not hydrogen bond with the carbonyl of Asp[177] in either the solution or crystal structures, thus reducing the length of strand V. The aspartic acid residues at the end of the fifth strand, together with Asp[107] and Trp[186], form a complex network of hydrogen bonds. The indole NH of Trp[186] is hydrogen bonded to the carbonyl of Asp[181], the NH of Asp[183] is bonded to the carboxylate of Asp[181] and the peptide NH of Trp[186] is bonded to the carboxylate of Asp[107].

Helix A, spanning Lys[110] to Glu[125], is mostly α-helix and both structures show the same hydrogen-bond patterns (Table 4). Notably, the NH of Trp[124] and Glu[125] share the carbonyl of Leu[121] as the same acceptor, and the indole NH proton of Trp[124] shows a hydrogen bond to

TABLE 4
HYDROGEN EXCHANGE AND HYDROGEN-BOND ANALYSIS OF sfSTR INHIBITED WITH *N*[1(*R*)-CARBOXYETHYL]-α-(*S*)-(2-PHENYLETHYL)GLYCINE-L-ARGININE-*N*-PHENYLAMIDE[a]

Donor atom	k_{hx} (s^{-1})[b]	Acceptor atom	NMR structure (Å)[c]	X-ray structure (Å)[c]	Secondary structure
Phe^{83}	nd	Asp^{237} $O^{\delta 1}$	–	2.0	
Arg^{84}	nd	–	–	2.1 (Wat^{337})	
Thr^{85}	20	–	–	–	
Phe^{86}	>20	–	–	2.4 (Wat^{514})	
Ile^{89}	nd	Phe^{86}	2.0±0.1 (30)	1.9	
Trp^{92}	<1	Tyr^{246} O^{η}	2.3±0.7 (21)	1.9	
Trp^{92} $N^{\varepsilon 1}H$	≪1	Ser^{206}	–	1.9	
Lys^{94}	≪1	–	–	–	
Thr^{95}	14	–	–	–	
His^{96}	<1	–	–	–	
Leu^{97}	≪1	Thr^{131}	1.9±0.1 (30)	2.0	S-1
Thr^{98}	≪1	Asp^{141} $O^{\delta 2}$	– (5)	2.0	
Tyr^{99}	≪1	Ser^{133}	2.2±0.3 (30)	2.3	S-1
Arg^{100}	≪1	Ile^{142}	2.0±0.1 (30)	2.1	S-1
Ile^{101}	<1	–	–	–	
Val^{102}	≪1	Ile^{144}	1.9±0.1 (30)	1.9	S-1
Val^{102}	≪1	Arg^{100}	–	2.4	
Asn^{103}	≪1	–	–	–	
Tyr^{104}	1	–	–	–	
Asp^{107}	≪1	Thr^{105}	1.9±0.1 (30)	–	
Asp^{107}	≪1	Thr^{105} $O^{\gamma 1}$	–	2.2	
Lys^{110}	<1	–	–	–	
Asp^{111}	2	–	–	–	
Ala^{112}	1	Pro^{109}	–	2.0	H-A
Val^{113}	≪1	Pro^{109}	2.2±0.1 (30)	2.2	H-A
Asp^{114}	≪1	Lys^{110}	2.2±0.1 (30)	1.9	H-A
Ser^{115}	≪1	Asp^{111}	1.9±0.1 (30)	2.1	H-A
Ala^{116}	≪1	Ala^{112}	2.4±0.1 (29)	2.3	H-A
Val^{117}	≪1	Val^{113}	2.5±0.1 (28)	2.2	H-A
Glu^{118}	≪1	Asp^{114}	1.7±0.1 (30)	2.0	H-A
Lys^{119}	≪1	Ser^{115}	1.8±0.1 (30)	1.8	H-A
Ala^{120}	≪1	Ala^{116}	1.8±0.1 (30)	2.1	H-A
Leu^{121}	≪1	Val^{117}	1.7±0.1 (30)	2.0	H-A
Lys^{122}	≪1	Glu^{118}	2.4±0.1 (18)	1.9	H-A
Val^{123}	≪1	Lys^{119}	1.8±0.1 (30)	2.1	H-A
Trp^{124}	≪1	Leu^{121}	2.1±0.1 (21)	2.1	H-A
Trp^{124} $N^{\varepsilon 1}H$	≪1	Ala^{200}	2.1±0.2 (29)	2.3	
Glu^{125}	≪1	Leu^{121}	2.0±0.2 (30)	2.0	H-A
Glu^{126}	≪1	Lys^{122}	2.3±0.2 (26)	2.0	
Val^{127}	≪1	Trp^{124}	1.8±0.1 (30)	2.4*	
Thr^{128}	<1	Glu^{125}	–	2.5	
Leu^{130}	≪1	Thr^{128} $O^{\gamma 1}$	–	2.5	
Thr^{131}	≪1	Thr^{95}	1.9±0.1 (30)	1.9	S-2
Phe^{132}	<1	–	–	2.1 (Wat^{432})	
Ser^{133}	≪1	Leu^{97}	2.1±0.3 (24)	2.3	S-2
Arg^{134}	<1	–	–	2.2 (Wat^{330})	
Leu^{135}	≪1	Tyr^{99}	2.8±0.2 (16)	2.2	S-2
Tyr^{136}	8	–	–	2.1 (Wat^{339})	
Glu^{137}	16				
Gly^{138}	9	–	–	1.9 (Wat^{518})	
Glu^{139}	8				
Ala^{140}	≪1	Met^{143} S^{δ}	– (3)	2.5[d]	
Asp^{141}	≪1	Thr^{98} $O^{\gamma 1}$	2.6±0.1* (3)	2.0	
Asp^{141}	≪1	Thr^{98}	–	2.3*	
Ile^{142}	≪1	Thr^{98}	1.8±0.1 (30)	2.0	S-3
Met^{143}	≪1	Asp^{177} $O^{\delta 1}$	– (4)	2.0	
Ile^{144}	≪1	Arg^{100}	1.9±0.1 (30)	1.9	S-3
Ser^{145}	≪1	Ala^{178}	2.1±0.2 (30)	2.4	S-3
Phe^{146}	≪1	Asn^{103} $O^{\delta 1}$	1.8±0.1 (30)	1.8	
Ala^{147}	≪1	Phe^{180}	2.1±0.2 (30)	1.8	S-3
Val^{148}	<1	–	–	2.4 (Wat^{354})	

TABLE 4
(continued)

Donor atom	k_{hx} (s^{-1})[b]	Acceptor atom	NMR structure (Å)[c]	X-ray structure (Å)[c]	Secondary structure
Arg^{149}	≪1	–	–	2.0 (Wat^{304})	
Glu^{150}	9				
His^{151}	6	–	–	2.0 (Wat^{303})	
His^{151} $N^{\delta 1}H$	nd	Arg^{149}	2.2±0.3 (28)	2.0	
Gly^{152}	>20	–	–	2.2 (Wat^{505})	
Asp^{153}	16				
Phe^{154}	>20	–	–	2.5 (Wat^{331})	
Tyr^{155}	≪1	Asp^{153} $O^{\delta 1}$	– (1)	2.1	
Phe^{157}	≪1	Arg^{149}	2.5±0.3* (9)	2.1	
Asp^{158}	<1	–	–		
Gly^{159}	≪1	–	–	2.0 (Wat^{304})	
Gly^{161}	nd	Glu^{184} $O^{\epsilon 1}$	– (15)	2.3	
Asn^{162}	<1	–	–	–	
Val^{163}	≪1	Asp^{158} $O^{\delta 2}$	–	2.2	
Leu^{164}	≪1	Inhibitor P1' (O)	3.0±1.5[e] (17)	1.8	
Ala^{165}	≪1	–	–	–	
His^{166}	≪1	His^{179}	2.0±0.2 (30)	1.9	S-5
Ala^{167}	<1	–	–	2.3 (Wat^{301})	
Tyr^{168}	≪1	Asp^{177}	2.9±0.3 (21)	2.1	S-5
Ala^{169}	<1	–	–	–	
Gly^{171}	3				
Gly^{173}	29				
Ile^{174}	18				
Asn^{175}	≪1	Pro^{172}	2.2±0.4 (23)	2.4	
Gly^{176}	2	–	–	–	
Asp^{177}	≪1	Ile^{174}	–	2.2	
Ala^{178}	≪1	Met^{143}	3.2±0.4* (2)	2.1	S-4
His^{179}	≪1	His^{166}	2.2±0.3 (23)	1.8	S-4
Phe^{180}	≪1	Ser^{145}	2.1±0.5 (26)	1.9	S-4
Asp^{181}	≪1	Leu^{164}	2.1±0.1 (30)	2.0	S-4
Asp^{182}	≪1	Ala^{147}	2.6±0.5 (11)	1.8	
Asp^{183}	≪1	Asp^{181} $O^{\delta 1}$	3.0±1.0* (14)	2.2	
Glu^{184}	≪1	Asp^{181}	–	2.3	
Gln^{185}	1	–	–	2.1 (Wat^{410})	
Trp^{186}	≪1	Asp^{107} $O^{\delta 2}$	–	1.9	
Trp^{186} $N^{\epsilon 1}H$	≪1	Asp^{181}	1.9±0.1 (30)	2.1	
Thr^{187}	≪1	Thr^{193}	2.7±0.3 (17)	2.1	
Lys^{188}	nd	–	–	2.1 (Wat^{363})	
Asp^{189}	<1	–	–	–	
Thr^{190}	>20				
Thr^{191}	15	Asp^{189} $O^{\delta 1}$	– (4)	2.2	
Gly^{192}	<1	Thr^{187} $O^{\gamma 1}$	– (8)	–	
Thr^{193}	1	Gln^{185}	–	1.9	
Asn^{194}	<1	Tyr^{223} O^{η}	2.4±0.6 (21)	2.1	
Leu^{195}	≪1	Thr^{187}	2.1±0.1 (30)	2.4	
Phe^{196}	≪1	–	–	–	
Leu^{197}	≪1	Asn^{194} $O^{\delta 1}$	2.2±0.6 (23)	2.0	
Val^{198}	≪1	Asn^{194}	2.4±0.1 (30)	2.4	H-B
Ala^{199}	≪1	Leu^{195}	1.7±0.1 (30)	1.9	H-B
Ala^{200}	≪1	Phe^{196}	2.0±0.2 (30)	1.9	H-B
His^{201}	≪1	Leu^{197}	2.7±0.2 (17)	2.0	H-B
His^{201} $N^{\delta 1}H$	nd	Leu^{218}	2.4±0.3 (30)	1.8	
Glu^{202}	≪1	Val^{198}	1.9±0.2 (30)	2.0	H-B
Ile^{203}	≪1	Ala^{199}	1.9±0.1 (30)	2.0	H-B
Gly^{204}	≪1	Ala^{200}	2.2±0.3 (22)	2.3	H-B
His^{205}	≪1	His^{201}	2.5±0.1 (30)	2.5	H-B
His^{205}	≪1	Glu^{202}	2.1±0.1 (19)	–	H-B
His^{205} $N^{\delta 1}H$	nd	Leu^{209}	2.9±0.3* (9)	2.0	
Ser^{206}	≪1	Glu^{202}	2.2±0.1 (30)	2.2	H-B
Leu^{207}	≪1	Ile^{203}	1.9±0.1 (30)	2.2	
Gly^{208}	≪1	Gly^{204}	2.3±0.4 (21)	–	
Gly^{208}	≪1	His^{205}	–	2.1	

TABLE 4
(continued)

Donor atom	k_{hx} (s^{-1})[b]	Acceptor atom	NMR structure (Å)[c]	X-ray structure (Å)[c]	Secondary structure
Leu^{209}	$\ll 1$	Gly^{204}	1.9 ± 0.2 (30)	1.9	
Phe^{210}	< 1	Arg^{84}	–	1.9	
Ser^{212}	$\ll 1$	Met^{219}	–	2.1	
Ala^{213}	3	–	–	2.0 (Wat^{362})	
Asn^{214}	8	Ser^{212} $O^{\gamma 1}$	– (2)	2.1	
Thr^{215}	1				
Glu^{216}	nd	Asn^{214} $O^{\delta 1}$	– (9)	2.0	
Ala^{217}	$\ll 1$	Asn^{214}	–	2.3	
Leu^{218}	< 1	Asp^{238} $O^{\delta 2}$	3.1 ± 0.9* (3)	2.1	
Met^{219}	$\ll 1$	Asp^{238} $O^{\delta 1}$	3.1 ± 0.5* (3)	2.0	
Tyr^{220}	$\ll 1$	Ala^{217}	–	2.0	
Leu^{222}	$\ll 1$	Tyr^{220}	2.4 ± 0.9 (19)	–	
Tyr^{223}	< 1	Inhibitor P2' (O)	–	1.9	
His^{224}	< 1	–	–	–	
Ser^{225}	21				
Leu^{226}	< 1	–	–	–	
Thr^{227}	> 20				
Asp^{228}	> 20				
Leu^{229}	10				
Thr^{230}	19				
Arg^{231}	15				
Phe^{232}	15				
Arg^{233}	< 1	–	–	–	
Leu^{234}	< 1	–	–	–	
Ser^{235}	$\ll 1$	Asp^{238} $O^{\delta 2}$	– (2)	2.0	
Gln^{236}	15				
Asp^{237}	12				
Asp^{238}	$\ll 1$	Ser^{235}	2.0 ± 0.1 (23)	–	
Asp^{238}	$\ll 1$	Ser^{235} $O^{\gamma 1}$	– (1)	2.2	
Ile^{239}	$\ll 1$	Ser^{235}	2.3 ± 0.1 (30)	2.3	
Asn^{240}	$\ll 1$	Gln^{236}	1.8 ± 0.1 (30)	1.9	H-C
Gly^{241}	$\ll 1$	Asp^{237}	2.7 ± 0.3 (18)	2.0	H-C
Ile^{242}	$\ll 1$	Asp^{238}	2.0 ± 0.2 (30)	2.2	H-C
Gln^{243}	nd	Ile^{239}	1.9 ± 0.1 (30)	2.0	H-C
Ser^{244}	$\ll 1$	Asn^{240}	2.3 ± 0.2 (18)	2.2	H-C
Ser^{244}	$\ll 1$	Gly^{241}	– (4)	2.4	H-C
Leu^{245}	$\ll 1$	Gly^{241}	2.1 ± 0.1 (30)	2.3	H-C
Tyr^{246}	$\ll 1$	Ile^{242}	2.6 ± 0.3* (4)	1.8	H-C
Tyr^{246} $O^{\eta}H$	nd[f]	Trp^{92}	2.6 ± 1.3 (23)		
Gly^{247}	$\ll 1$	Gln^{243}	–	1.9	
Asp^{251}	14				
Ser^{252}	23				
Glu^{254}	18				
Thr^{255}	1				
P1' (NH_2)	nd	Ala^{165}	2.6 ± 0.9 (18)	2.2	
P2' (NH)	4	–	–	–	
P3' (NH)	< 1	Asn^{162}	2.0 ± 0.1 (26)	2.0	

[a] Unless indicated otherwise, the donor and acceptor atoms are the peptide NH and C'O, respectively. Interactions that involve side-chain NH protons are not included, except for tryptophan and histidine, which appear to be slowly exchanging. In the crystal structure a number of water molecules are indicated as acceptors.

[b] The exchange rate of the donor NH (k_{hx}) is divided into three groups: $\ll 1$ s^{-1}, a ^{15}NH correlation is observed in experiments with the protein in 100% D_2O buffer; < 1 s^{-1}, a peak was not observed in the preceding experiment, but showed minimal intensity changes in saturation transfer experiments; for rates > 1 s^{-1}, intensity changes were measured in saturation transfer experiments; nd, not determined because the resonance was either overlapping or not observable.

[c] Distance between the NH proton and the acceptor atom. The hydrogen-bond energy was less than −1.0 kcal/mol, except where indicated (*) where the energy was between −0.5 and −1.0 kcal/mol. For the solution structure, the number of structures (maximum of 30) where the hydrogen-bond energy is less than −1.0 kcal/mol is included in parentheses.

[d] The expected distance for a hydrogen bond between the S^{δ} of a methionine and an NH is 2.6 Å.

[e] This hydrogen bond is long, with a large standard deviation in the solution structure, because the peptide bond between P1' and P2' rotates by ~180° in 11 out of the 30 solution structures compared to the crystal structure.

[f] Tyr^{246} H^{η} is observed at 10.24 ppm in ^1H spectra.

the carbonyl of Ala[200], which would, in addition to the hydrophobic contacts between helices A and B, stabilize the interaction between these helices. In solution, the two residues following this helix, Thr[128] and Pro[129], show a small amount of cis/trans isomerism, as indicated by strong NOEs from the $C^{\alpha}H$ of the threonine to the $C^{\delta}H$ of the proline and a weak $C^{\alpha}H$-$C^{\alpha}H$ NOE (not shown). All NOEs that can be assigned to the cis form have been excluded from the structure calculations; however, unintentional inclusion of NOEs of this form may be responsible for the differences observed between the solution and crystal structures for this region and its interaction with the C-terminal region, Pro[248]–Pro[249] (Table 2).

Helix B, the catalytic helix, is also predominantly an α-helix, spanning Leu[195]–Ser[206]. Similar features are observed in both the solution and crystal structures. The helix is N-capped by a hydrogen bond between the NH of Leu[197] and the side-chain amide oxygen of Asn[194]. In the consensus region HEIGH of the solution structure, which is common to all metzincins and thermolysin (Bode et al., 1993), the hydrogen-bond partner of the NH of His[205] appears to be the carbonyl of His[201], with some tendency to Glu[202] (see Table 4 and Fig. 5), thus creating an ambiguity in determining if this part of the helix is α or 3_{10}. In the crystal structure the hydrogen bond between His[205] and His[201] is favored energetically (–1.2 kcal/mol), despite the fact that the distance between the NH proton and the carbonyl is 2.50 Å. The distance between the NH of His[205] and the carbonyl of Glu[202] is shorter (2.35 Å) but the angle is poor, resulting in a hydrogen-bond energy of –0.1 kcal/mol. These data suggest that this region of helix B is slightly distorted from an ideal α-helix in both the solution and crystal structures. This distortion is also observed in thermolysin (3tln) (Holmes and Mathews, 1982), fibroblast (1hfc) and neutrophil collagenase (1mnc) (Spurlino et al., 1994; Stams et al., 1994) (Fig. 5). The $N^{\delta 1}H$ proton of His[201] is hydrogen bonded to the carbonyl of Leu[218] in both structures and the $N^{\delta 1}H$ of His[205] is hydrogen bonded to the carbonyl of Leu[209] in the crystal structure, but not in the solution structure. The $N^{\delta 1}H$ of His[211] points towards the solvent and is not hydrogen bonded. In the solution structure, Gly[208] is predicted to hydrogen bond Gly[204], thus extending helix B, whereas in the crystal structure it hydrogen bonds the amide of His[205], forming a 3_{10} turn.

Helix C, spanning Gln[236] to Tyr[246], is completely α-helical in the crystal structure, whereas in the solution structure this helix is slightly ill-formed, a problem that reflects the lack of short-range NOE data (Gooley et al., 1993). The solution structure shows it is α-helix from the carbonyl of Ser[235] to the NH of Tyr[246]. Both the NH of Asp[238] and Ile[239] show hydrogen bonds to the carbonyl of Ser[235] in this structure, whereas these atoms display hydrogen bonds to the O^{γ} and carbonyl of Ser[235], respectively, in the crystal structure.

β-turns and Ω-loop

The solution and crystal structures have two 1-4 turns in common: Phe[86]–Ile[89] (type II) and Pro[172]–Asn[175] (type II'). The first turn is not predicted to be type II in the solution structure, because Gly[88] remains unassigned. The φ,ψ angles of Ile[89] are unusual for both the solution and crystal structure, placing this residue in the region of left-handed helix in the Ramachandran plot (Fig. 4). Both structures show an Ω-loop (Leszczynski and Rose, 1986) encompassing Thr[187]–Leu[195], which is stabilized by hydrogen bonds between the NH of Leu[195] and the carbonyl of Thr[187], and between the NH of Thr[187] and the carbonyl of Thr[193].

The crystal structure shows three additional 1-4 turns, all of type I: Asp[181]–Gly[184], Asn[214]–Ala[217] and Ala[217]–Tyr[220]. In the solution structure, the Kabsch–Sander predictions describe these turns as bends, which is borne out by the poor hydrogen-bond energies (Table 4). The φ,ψ angles, NOE patterns and slowly exchanging amide protons support the presence of the turns; however, the data are incomplete, with few short-range NOEs, and the resonances of the NH of Met[219] and Tyr[220] overlap, thus these turns are not well determined. Two additional interactions stabilize the turn Ala[217]–Tyr[220]: hydrogen bonds from the buried carboxylate of Asp[238] to the NH of Leu[218] and Met[219]. This structural feature has been observed in the crystal structure of the collagenases and is likely to be common amongst the MMPs. These bonds are weakly predicted in the solution structure compared to the crystal structure (Table 4).

Irregular loops and other interactions

Three regions of sfSTR that do not belong to regular secondary structures are of particular interest. They are irregular loops that contain NH protons exhibiting fast exchange with water (Table 4), and appear structurally and/or functionally important. The first of these spans 15 residues, from the NH of Val[148] to the carbonyl of Val[163], and joins strands III and IV (Fig. 6). It crosses over strand V of the β-sheet and contains two of the structural zinc ligands, His[151] and Asp[153], and four residues that ligate calcium, Asp[158] ($O^{\delta 1}$), Gly[159] (O), Gly[161] (O) and Val[163] (O) (Becker et al., 1995). Two other residues, Asp[181] ($O^{\delta 1}$) and Glu[184] ($O^{\varepsilon 2}$), also ligate this calcium. Notably, residues at either end of this loop, Arg[149] and Asn[162], show unusual φ angles, locating these residues in the right-hand side of the Ramachandran plot (Fig. 4). The $N^{\delta 1}H$ proton of His[151] is hydrogen bonded to the carbonyl of Arg[149] in both the solution and crystal structures. The protonated ring nitrogens of His[166] and His[179], the other two structural zinc ligands, are not hydrogen bonded in the solution structure, but are hydrogen bonded to water in the crystal structure. A second loop spanning nine residues (Fig. 6), extending from the carbonyl of Tyr[168] to the NH of Asp[177], ligates a second calcium: Gly[173] (O),

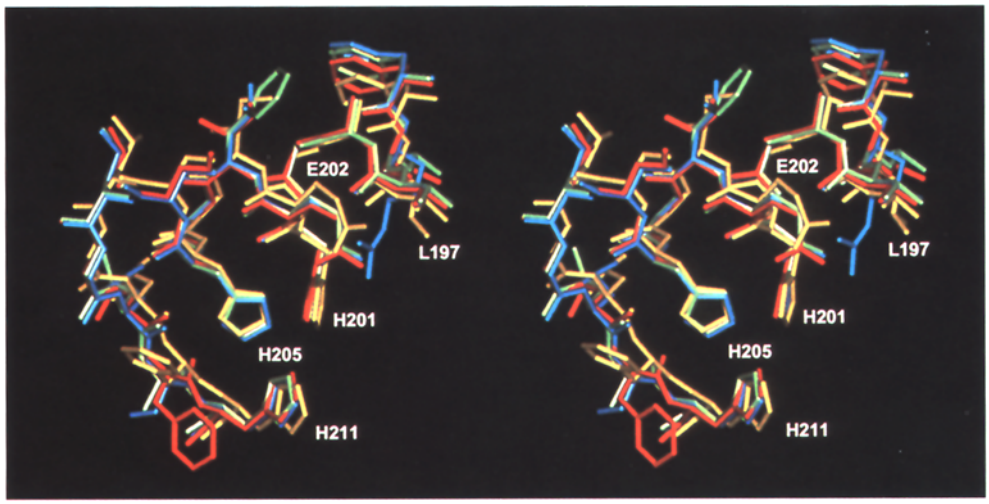

Fig. 5. Superposition of the segment Phe[196]–His[211] of a member of the family of solution structures of sfSTR (yellow) and the crystal structure of sfSTR (red), and the same region of neutrophil collagenase, 1mnc (green) and fibroblast collagenase, 1hfc (blue). The structures have been superimposed on the region Leu[197]–His[205] for minimal rmsd. All structures are similar in the consensus region HEXXH, and include a long hydrogen bond from His[205] to His[201] (numbering of sfSTR). Note that the equivalent residue of Leu[197] in sfSTR is an arginine in fibroblast collagenase. This arginine delimits the S1' subsite in the latter enzyme.

Asn[175] (O) and Asp[177] ($O^{\delta 1}$). Residue Asp[141] (O) also ligates this calcium.

The solution structures were calculated without calcium. For the first well-defined calcium site, Asp[158]–Val[163], the rmsd of the solution structures to the crystal structure are greater than the average values of 1.51 Å for backbone heavy atoms and 2.18 Å for all heavy atoms in the segment Asp[158]–Pro[160] (1.58–2.07 Å; 1.69–4.02 Å) and less than average for Gly[161]–Val[163] (0.56–0.81 Å; 0.49–1.87 Å). In the family of solution structures the region Asp[158] to Pro[160] is poorly defined, showing an rmsd > 1.35 Å (backbone atoms), whereas Gly[161]–Val[163] is well defined (rmsd < 0.79 Å). The rmsd values of the solution structures to the crystal structure for the second site are 1.73–2.07 Å (backbone atoms) and 1.91–2.09 Å (all heavy atoms) for Gly[173]–Ile[174], and 0.71–1.27 Å (backbone atoms) and 0.86–1.75 Å (all heavy atoms) for Asn[175]–Asp[177]. This second site is well defined for the family of solution structures (rmsd < 0.82 Å). The other three residues that ligate these two calciums, Asp[141], Asp[181] and Glu[184], are similar in the crystal and solution structures (Fig. 6) and are well defined in the solution structure. For both sites, the residues that show the largest rmsd values are characterized by sequential, but not by short- or long-range NOEs. Particularly notable is Asp[158], which shows an rmsd of 4.02 Å (all heavy atoms) for the solution to the crystal structure (Fig. 6) and shows only several sequential NOEs. The crystal structure suggests that short-range NOEs are expected between the $C^{\beta}H_2$ protons of Asp[158] and of Asn[162] (4–5 Å); however, these NOEs were not observed.

A third loop of 17 residues extends from Pro[221] to Asp[238]. Residues in this loop form a part of the upper lip of the S1' subsite (Pro[221]–Tyr[223]) and the S1' subsite itself (Tyr[223]–Leu[226]). The structure of the region His[224]–Arg[231] differs significantly between the solution and crystal struc-

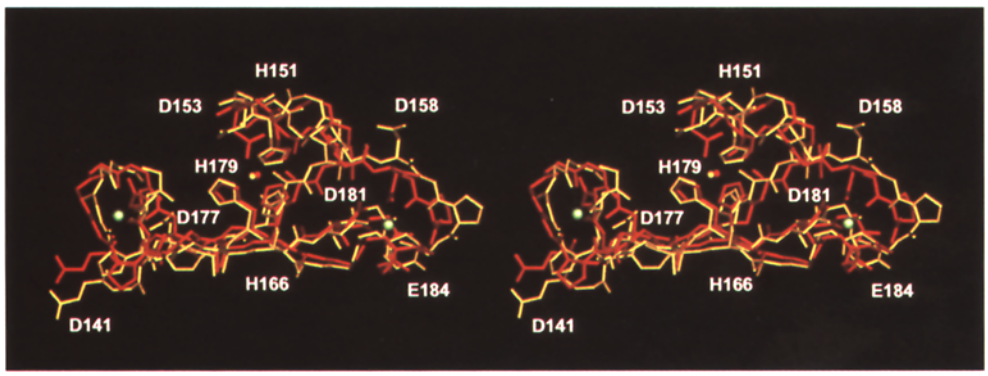

Fig. 6. Superposition of the regions Asp[141]–Glu[184] of the crystal and of a member of the family of solution structures of inhibited sfSTR. These regions include the two well-defined calcium binding sites observed in the crystal structure. The side chains of the residues that ligate zinc and calcium are shown.

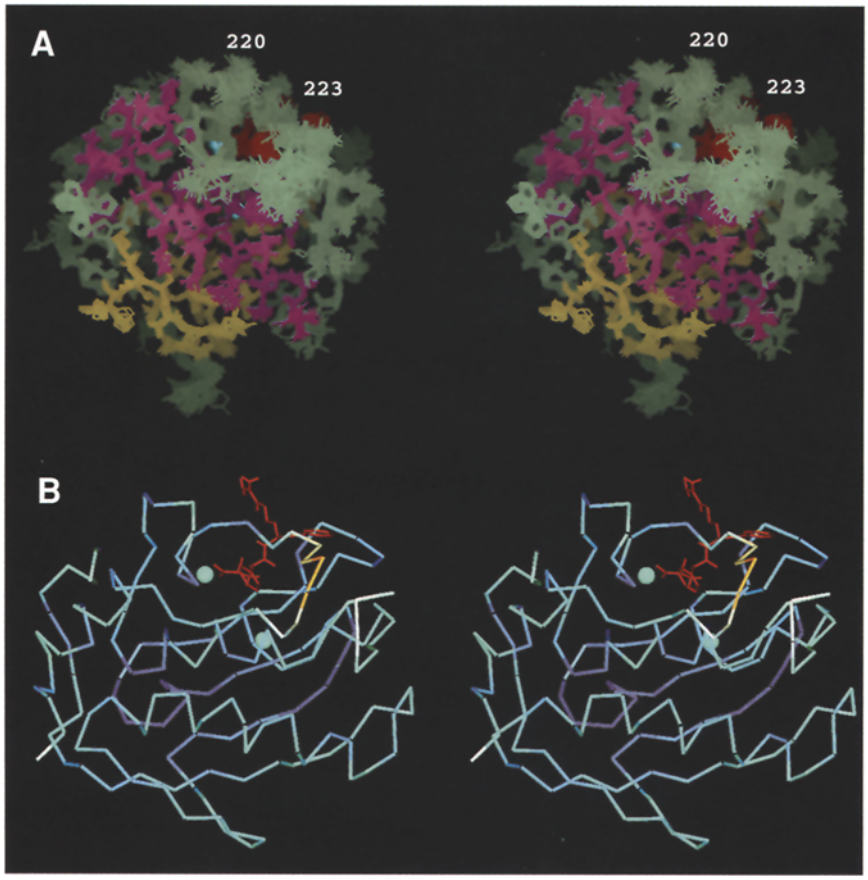

Fig. 7. (A) Superposition of the 30 solution conformers of inhibited sfSTR from residues 83–250. All heavy atoms are shown. Helices are colored magenta, β-sheets are in yellow, irregular structure is in gray, zinc is in cyan and the inhibitor is shown in red. The structures are viewed from below the S1' subsite. In this orientation the P1' group can be observed, showing that this subsite has no bottom. The well-ordered secondary structure is clear, and the disorder of the residues in the region His^{224}–Arg^{231} surrounding the S1' subsite is also apparent. (B) The same orientation for the crystal structure shows the bottomless S1' subsite. The protein is colored according to B-factor, where blue is small and yellow is large. The inhibitor is in red and the zinc atoms are in cyan.

tures (Fig. 3). In the solution structure, this region is poorly characterized by long-range NOEs: residues His^{224}, Leu^{226}, Thr^{227}, Thr^{230} and Arg^{231} show no long-range NOEs. The lack of NOEs results in large rmsd values (> 2 Å) for the residues His^{224} to Arg^{231} and suggests that the backbone and side chains of these residues are flexible. In some cases the lack of NOEs is due to spectral problems, for example, resonances of Leu^{226} overlap with those of Leu^{229} and the ring protons of His^{224} are unassigned. Thus, the large rmsd values may be due to a lack of data rather than mobility. In the crystal structure, however, the temperature factors of residues 224–231 are significantly higher (22.8 $Å^2$) than those of the average protein atoms (11.5 $Å^2$), supporting a flexible structure. There are few intermolecular lattice-specific contacts involving this region, indicating that the conformation observed in the crystal structure is probably not an artifact of crystallization. Only residues Leu^{222}–His^{224}, Arg^{231} and Arg^{233} show contacts of < 4 Å with protein groups from neighboring molecules in the crystal lattice. The difference between the solution and crystal structures may be further exacerbated by NOE weighting. The sequential connectivities of Tyr^{223}–Leu^{226} are characterized by $d_{\alpha N}$ NOEs and therefore this region appears extended in the solution structure. The $d_{\alpha N}$ NOE is often observed for flexible peptides or regions of a protein, whereas the mutually exclusive d_{NN} NOE that would support mobility may not be observed; therefore the structure is weighted towards an extended conformer (note that only $d_{\alpha N}$ NOEs are observed in the disordered C-terminal tail of sfSTR). These mutually exclusive NOEs have only been observed between Arg^{231} and Phe^{232}. The most significant differences between the solution and crystal structures for this loop are observed in the ϕ,ψ angles of residues Ser^{225} and Leu^{226}: $-126° \pm 26°, 160° \pm 19°$ and $-127° \pm 30°, 148° \pm 10°$, respectively, for the solution structure and −56°,98° and −67°,127°, respectively, for the crystal structure. For these residues the ϕ,ψ angles of the crystal structure are compatible with the NOE data (suggesting an extended structure). All residues in the 220s, except for Arg^{229}, were constrained by experimental ϕ,ψ angles. The experimental ψ angle restraint of Ser^{225} is 135°–185° and that of the ϕ

angle of Leu^{226} is $-155° - -75°$, i.e., these ranges do not include those of the crystal structure. The angle constraints were objectively derived from sequential, intraresidue and $^3J_{NH\alpha}$ data using the program HABAS and thus these angle differences emphasize the difficulty in using NOE-weighted distances to adequately define, or in this case prevent over-defining, a flexible region.

Another irregular region that differs between the two structures is the N-terminal segment Phe^{83}–Gly^{88}, which may play an important functional role in catalysis. An N-terminally truncated form of neutrophil collagenase was shown to be less active than the full-length protein (Bode et al., 1994). Comparison of the crystal structure of this protein with the wild type shows that the truncated form lacks a salt link between the N-terminus and the carboxylate of the conserved Asp^{232}. This salt link is observed in the crystal structure of sfSTR, but it is not always apparent in the solution structure. The distances between the N-terminus and the two oxygens of the carboxylate of Asp^{235} are 5.7 ± 2.0 Å and 5.3 ± 1.4 Å, ranging from 2.7 to 11 Å for the 30 conformers. The spin system of Gly^{88} is completely unassigned and that of Pro^{87} is poorly assigned (see the supplementary material), and although long-range NOEs have been found for the side chains of residues Phe^{83}, Arg^{84} and Thr^{85} (to Leu^{209}, Phe^{210}, Asn^{240}, Ser^{244} and Leu^{245}), there are few sequential NOE assignments and therefore the backbone of Phe^{83}–Gly^{88} in the solution structure is poorly defined. Two NH protons are difficult to observe, Arg^{84} has not been assigned and Phe^{86} is very weak. Thus, the absence of NOEs in this region may, in part, be due to conformational averaging or rapid exchange with water.

Inhibitor conformation and intermolecular contacts

The inhibitor binding sites of the solution (Gooley et al., 1994) and the crystal (Becker et al., 1995) structures have been previously described. The difference between the initial solution structure and that presented here is the bottomless S1' subsite (Fig. 7) and is due to misassignment of the side chains of Leu^{218} and Leu^{226} in the initial structure. This bottomless subsite is apparent in the crystal structures of sfSTR and neutrophil collagenase, but not in that of fibroblast collagenase. In the latter protein Arg^{214} delimits the S1' subsite, whereas the equivalent residue in sfSTR, Leu^{197}, is on the edge of the S1' subsite and, as indicated by intense intraresidue NOEs between both $C^{\delta}H_3$ and the $C^{\alpha}H$ proton, appears flexible.

The ϕ,ψ angles for the P1' and P2' groups of the inhibitor in the crystal and solution structures are, respectively, $-107.9°,142.4°$ and $-83.7° \pm 6.3°,190.2° \pm 90.0°$ for P1' and $-91.5°,152.3°$ and $-162.9° \pm 88.6°,121.9° \pm 18.6°$ for P2'. The poorly defined ψ of P1' and ϕ of P2' of the solution structure are due to the absence of NOEs from the NH of P2' to the protein and the presence of only one weak sequential NOE (the NH of P2' to the $C^{\alpha}H$ of P1'). This lack of NOE data results in a poorly defined structure around P2'. For example, the distance between the NH of P2' and $C^{\alpha}H$ of P1' is 2.7 ± 0.6 Å and 11 of the 30 solution structures show the peptide bond between P1' and P2' rotated by ~180° relative to the crystal structure. The well-defined ϕ angle for P3' is due to a strong sequential NOE between the NH of P3' and the $C^{\alpha}H$ of P2' as well as many NOEs from the P3' NH to the protein. Thus, the local structure around P3' is well defined; for example, the distance between the NH of P3' and the $C^{\alpha}H$ of P2' is 2.3 ± 0.1 Å. This difference in well and poorly defined structure affects the interpretation of hydrogen bonds between the inhibitor and the protein.

There are two regions of protein backbone that can form hydrogen bonds to the backbone atoms of the inhibitor: Asn^{180}–Ala^{165} and Pro^{221}–Tyr^{223}. The segment Asn^{180}–Ala^{165} shows the same hydrogen bonds in both the solution and crystal structures (Table 4): from the carbonyl of Ala^{165} to the amine of P1', the carbonyl of Asn^{162} to the NH of P3' and the NH of Leu^{164} to the carbonyl of P1'. For the region Pro^{221}–Tyr^{223} the crystal structure shows a hydrogen bond, which is not observed in the solution structure, between the NH of Tyr^{223} and the carbonyl of P2'. The absence of this hydrogen bond in the solution structure is particularly interesting, as it has been observed in all crystal structures of MMPs that have been reported. Since few NOEs between the backbone atoms of the inhibitor and the segment Pro^{221}–Tyr^{223} are observed, it is not surprising that the hydrogen bond is not predicted. In several, but not all, inhibited collagenase structures, a hydrogen bond has been observed between the P2' NH and the carbonyl of the equivalent residue to Pro^{221}. Neither the crystal nor the solution structure of inhibited sfSTR shows this hydrogen bond and its absence is supported by the amide having an exchange rate that is relatively faster than the exchange rates of the other NH protons involved in hydrogen bonds to the inhibitor (Table 4).

The NH protons that form hydrogen bonds between the amide and carbonyl atoms of sfSTR are almost all slowly exchanging ($\ll 1\ s^{-1}$). Of the three hydrogen bonds that involve the carbonyl and NH of the protein and the inhibitor, only the NH of Leu^{164} is slowly exchanging, whereas the NH of Tyr^{223} and of the P3' of the inhibitor are relatively fast ($< 1\ s^{-1}$). The NH exchange rate for these groups may be due to protection by a hydrogen bond, solvent accessibility and a third phenomenon, the off-rate (k_{off}) of the inhibitor, which in this case is $10^{-3}\ s^{-1}$ (Izquierdo-Martin et al., 1994). This off-rate is similar to the minimal NH exchange rates that could be measured in a hydrogen–deuterium exchange experiment and thus may significantly attenuate the NH exchange rates. The protection of the NH of Leu^{164} may be due predominantly to a hydrogen bond and lack of solvent penetration. Solvent accessibility analysis shows that in the presence of

TABLE 5
INTERMOLECULAR CONTACTS BETWEEN *N* [1(*R*)-CARBOXYETHYL]-α-(*S*)-(2-PHENYLETHYL)GLYCINE-L-ARGININE-*N*-PHENYLAMIDE AND sfSTR[a]

Inhibitor	NMR and X-ray[b]	NMR[c]	X-ray[d]
P1' C^{β}	His^{201} $C^{\delta2}$,$N^{\epsilon2}$	Leu^{164} $C^{\delta1}$ His^{201} C*,$N^{\delta1}$,$C^{\epsilon1}$	Glu^{202} $O^{\epsilon2}$
P1' C^{γ}		Tyr^{220} O	Pro^{221} O Tyr^{223} N
P1' C^{δ}	His^{201} C^{γ},$N^{\delta1}$ Tyr^{223} N,C^{α}	Tyr^{220} O	Tyr^{223} C^{β}
P1' $C^{\epsilon1,\epsilon2}$	Val^{198} $C^{\gamma2}$ His^{201} C^{β},C^{γ},$N^{\delta1}$,$C^{\epsilon1}$ Tyr^{220} O Leu^{222} C,O Tyr^{223} N,C^{α},$C^{\delta1}$	Leu^{164} $C^{\delta1}$ Leu^{218} O*	Val^{198} C^{α} Tyr^{223} C^{β}
P1' $C^{\zeta1,\zeta2}$	Leu^{197} C,O Val^{198} C^{α},$C^{\gamma2}$ His^{201} $N^{\delta1}$ Leu^{218} O Tyr^{220} O Tyr^{223} C^{α},$C^{\delta1}$	Leu^{197} $C^{\delta2}$ Leu^{218} C Leu^{222} O* Tyr^{223} C^{γ}* His^{224} N	His^{201} C^{β},C^{γ}
P1' C^{η}	Leu^{197} O Tyr^{223} C^{α}	Leu^{197} C^{γ},$C^{\delta1}$,$C^{\delta2}$	His^{201} C^{β}
P3' C^{α}	Asn^{162} O Leu^{164} C^{γ},$C^{\delta1}$	Asn^{162} N Leu^{164} $C^{\delta2}$*	
P3' $C^{\beta1,\beta2}$	Asn^{162} O Leu^{164} C^{γ},$C^{\delta2}$ Tyr^{223} C^{β}	Asn^{162} N* Leu^{164} $C^{\delta1}$*	Tyr^{223} C,O,$C^{\delta2}$
P3' $C^{\gamma1,\gamma2}$		Tyr^{223} C^{β}*	Tyr^{223} C,O,$C^{\delta2}$

[a] Contacts are listed between the heavy atoms of the inhibitor and the protein for distances less than 4.5 ± 0.5 Å and 4.0 Å, in the solution and crystal structures, respectively. As the side chain of P2' is flexible, contacts are not listed. The nomenclature for the inhibitor atoms is described in Fig. 8B.

[b] The protein atom shows a contact to the inhibitor atom in both the solution and crystal structures.

[c] Contacts in the solution structure only. Atoms marked (*) are 4.0–4.5 Å between the inhibitor and the protein atom in the crystal structure.

[d] Contacts in the crystal structure only.

the inhibitor this NH proton is inaccessible, and in the absence of the inhibitor (determined by removing the inhibitor in the crystal structure), it is slightly accessible (5 $Å^2$). Removal of the inhibitor by this method does not account for conformational changes that may influence the exchange rates of the NH protons in the inhibitor-free state. The relatively fast exchange rates of the NH of P3' and Tyr^{223} are probably influenced by hydrogen bonds and the k_{off} rate of the inhibitor. Notably, in the absence of the inhibitor the NH of Tyr^{223} is relatively exposed, 10 $Å^2$, and thus its exchange rate may not be limited by solvent accessibility.

The protein–inhibitor contacts of the solution and crystal structures of sfSTR are summarized in Table 5 and Fig. 8. Of the 71 intermolecular NOEs, five are violated by more than 0.5 Å in the crystal structure: $C^{\gamma1}H$ of Val^{163} to $C^{\beta}H$ of P2'; $C^{\delta1}H$ of Leu^{222} to $C^{\beta}H$ of P3'; and $C^{\gamma}H$, $C^{\delta1}H$ and $C^{\delta2}H$ of Leu^{197} to $C^{\eta}H$ of P1'. Two of the latter are violated by more than 2 Å (Table 2). In general, however, the same conclusions can be drawn: the P1' side chain binds in a deep hydrophobic subsite, with contacts to the side chains of Val^{198}, His^{201} and Tyr^{223}; the S2' subsite is nondescript, with the P2' residue exposed to solvent; the S3' subsite is hydrophobic, consisting of leucine and tyrosine side chains; and the P3' group extends into solvent. In specific terms, there is a set of atoms in common between the two structures; particularly notable are the carbonyl oxygens of several residues of the protein (Table 5), which offer potential hydrogen-bond acceptors. There are, however, atoms showing contacts in the solution structure that are not present in the crystal structure and vice versa, e.g., in the crystal structure Pro^{221} and Tyr^{223} show contacts to the ethylene group of P1' that are not observed in the solution structure; the side-chain atoms of Leu^{197} show contacts to C^{η} of P1' in the solution structure (3.5 ± 0.4 to 4.1 ± 0.5 Å), whereas these atoms are approximately 5.5 Å apart in the crystal structure (Table 2). It is important to discuss whether these differences would affect the interpretation of the role of these residues in mechanism, substrate binding or, particularly, in inhibitor design. For the first example, the lack of contact from Pro^{221} and Tyr^{223} to the inhibitor in the solution structure is consistent with the absence of hydrogen bonds between the inhibitor and this region, suggesting that an inhibitor without these hydrogen bonds may not be significantly less potent. However, the crystal structure contradicts this conclusion and indicates that the loss of the hydrogen bond between the P3' carbonyl and the NH of Tyr^{223} may result in loss of potency. The second example is less clear. Despite the difference (~2 Å) between the relative positions of the side-chain atoms of Leu^{197} to the inhibitor in the two structures, the residue is observed to be on the edge of the S1' subsite and, as the side chain of this residue is mobile, it would not interfere with larger P1' groups and thus in both structures appears to play a passive role in providing a hydrophobic surface.

The orientation of the P1' group is similar in both the crystal and solution structures: the χ^1 and χ^2 angles are −180° and 175°, respectively, in the crystal structure and −137° ± 39° and 174° ± 26°, respectively, in the solution structure. In the crystal structure the ring of the P1' group is located in a narrow bottleneck, similar to the crystal structure of neutrophil collagenase complexed with a peptide hydroxamate (Grams et al., 1995). The NMR

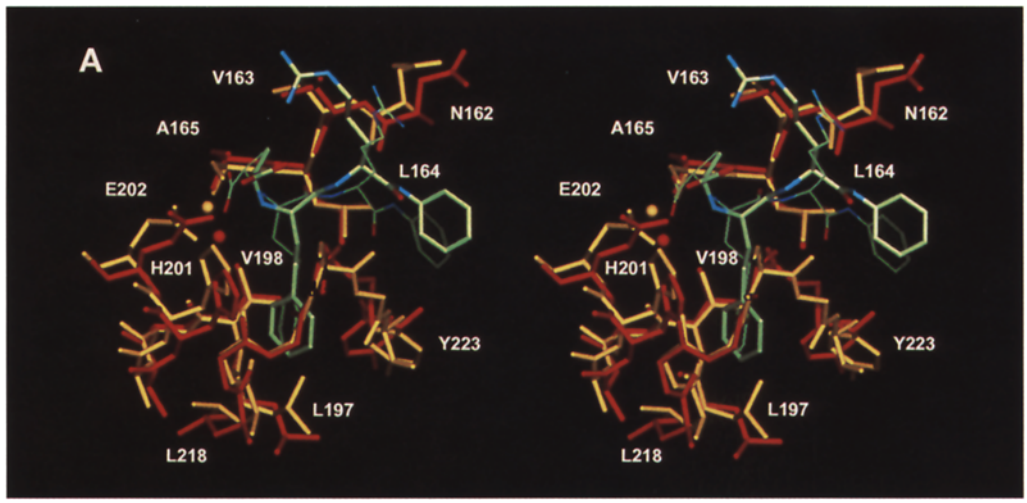

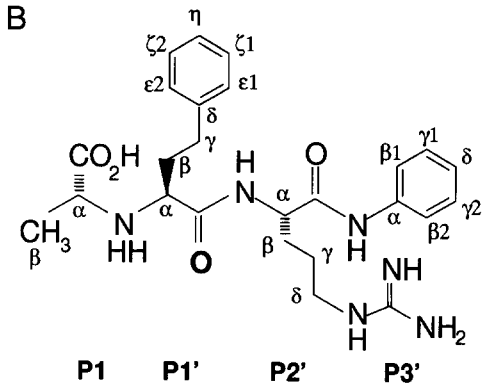

Fig. 8. (A) Superposition of the inhibitor binding site, showing protein residues that are in intermolecular contact with the inhibitor of the crystal structure and a representative member of the family of solution structures of inhibited sfSTR. The crystal structure is shown in red and its inhibitor in thin lines, and the solution structure in yellow and its inhibitor in thick lines. (B) Schematic of the inhibitor *N*[1(*R*)-carboxyethyl]-α-(*S*)-(2-phenylethyl)glycine-L-arginine-*N*-phenylamide.

spectra of this ring show degenerate chemical shifts for the two pairs of ring protons, $C^{\varepsilon 1}H$ and $C^{\varepsilon 2}H$ at 6.92 ppm, and $C^{\zeta 1}H$ and $C^{\zeta 2}H$ at 7.46 ppm, suggesting that at 40 °C the flip rate of this ring is fast. Under the solution conditions of the present work only one aromatic ring, Phe[157], in sfSTR is slowly flipping. Therefore it can be concluded that there are motions within the S1' pocket of sufficiently large amplitudes to allow the P1' ring to undergo 180° flips.

Solvent accessibility and interaction with water

The total accessible surface for the crystal structure is 9342 Å^2 and for the solution structure it is 9269 ± 120 Å^2, suggesting that the latter structure is slightly, but not significantly, more compact. In Fig. 9 the accessible surface of the nitrogen atoms is plotted for both structures. The most accessible nitrogens are found in the N-terminal segment Phe[83]–Thr[95], the outer β-strand Phe[132]–Glu[139], and segments that join the regular elements of secondary structure: Tyr[104]–Asp[111], Val[148]–Asn[162], Ala[169]–Ile[174], Gln[185]–Thr[190], Ala[213]–Leu[218] and His[224]–Asp[237]. Generally, amide protons that show fast exchange (> 1 s^{-1}) are not hydrogen bonded and are accessible to solvent, whereas amide protons that are in slow exchange are buried and hydrogen bonded. There are several instances where these generalizations are contradicted. Thr[230]–Phe[232], which is a part of an irregular loop in the crystal and solution structures, is not accessible to solvent, despite the fact that all three amides show fast rates of exchange. The presence of $d_{\alpha N}$ and d_{NN} NOEs between Arg[231]–Phe[232] shows this region to be mobile, and therefore the static representation of the structures belies its true mobility. Asn[103], Ala[140], Arg[149], Gly[159], Ala[165] and Phe[196] show slow exchange rates (≪ 1 s^{-1}) with solvent, but are not predicted to be involved in hydrogen bonds with carbonyl groups in either the solution or the crystal structure (Table 4). Asn[103] and Ala[165] are buried and inaccessible to solvent. Ala[140] appears to form a hydrogen bond with the S^{δ} of Met[143]. The hydrogen-bond geometry (Gregoret et al., 1991) between the latter atoms is well satisfied in the crystal structure and, although the geometry is less well satisfied in the solution structure, there is no other potential acceptor of the slowly exchanging amide proton of Ala[140]. Arg[149] and Gly[159] are inaccessible to solvent, but

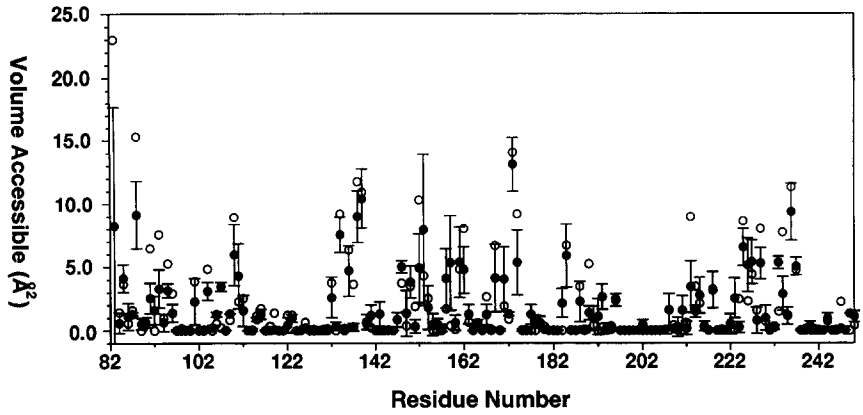

Fig. 9. Solvent accessibility of the nitrogen atoms of inhibited sfSTR for residues 83–250. The solution structure is represented by (●) and the crystal structure by (○).

hydrogen bonded to a water molecule in both the solution and crystal structures (see below). The NH of Phe[196] points towards the solvent and is weakly accessible to solvent (~2 Å^2). This residue, however, lies in a groove in the protein and is probably protected by the tertiary structure.

To determine the presence of bound water in the solution structure, water-selective 2D heteronuclear spectra were acquired. In these difference spectra, peaks are solely due to NOEs and ROEs to the resonance at the water frequency. In Fig. 10 water-selective 2D ^{15}N and ^{13}C ROE-HSQC spectra are shown. Peaks that show positive ROEs may be spatially near (<4 Å) bound water, whereas a negative ROE indicates an indirect interaction, such as chemical exchange. A positive ROE, however, may also be due to a ROE to protons of groups that are in rapid exchange with water and that resonate at the water frequency, for example the OH of serine, threonine and tyrosine. Exclusion of these interactions suggests that there are two tightly bound water molecules in common in the crystal and solution structures. There are an additional 38 water molecules in the crystal structure that participate in hydrogen bonds with the protein, and as most of these interact with mobile polar side chains that are on the surface of the protein, these waters are generally not expected to be observed in the solution structure. Strong positive ROE peaks were observed from His[151], Asp[153] and Tyr[155] to water (equivalent to Wat[303] of the crystal structure) (Fig. 10A). These amides also show strong negative NOEs, and these NOEs were attenuated at least 15-fold in control spectra. The strong positive ROE and negative NOE indicate a residence time of

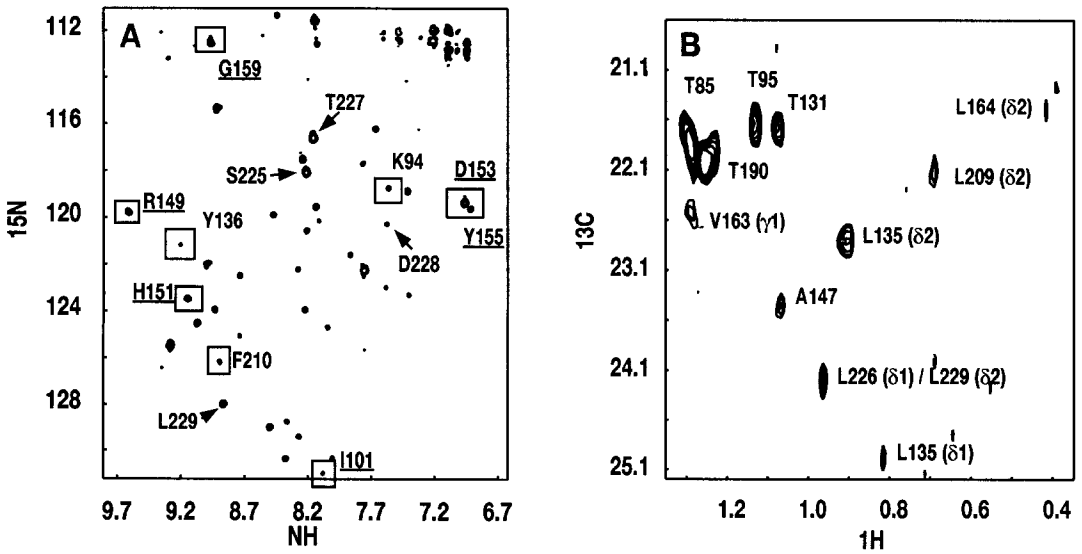

Fig. 10. Regions of the (A) 2D H_2O-ROE ^{1}H,^{15}N HSQC and (B) 2D H_2O-ROE ^{1}H,^{13}C HSQC spectra of inhibited sfSTR. In (A) residues that show a positive ROE and a negative NOE to water and are significantly attenuated (greater than 11-fold) in control spectra are boxed and underlined. Peaks that are not attenuated in control spectra, whose protons are not near an exchangeable proton, are boxed. Ser[225], Thr[227], Asp[228] and Leu[229] show strong negative ROEs. For clarity, all other positive ROEs that were assigned to an NH proton near an exchangeable group are not labeled. In (B) all peaks are positive ROEs. All these peaks showed negative NOEs, but all except Leu[226]/Leu[229] displayed little attenuation in control experiments. Most of these protons are near exchangeable protons.

> 500 ps (Otting et al., 1991). In the crystal structure this water is hydrogen bonded to the NH of His^{151} and the carbonyl of Asp^{153}. The NH of Arg^{149} and Gly^{159} also showed strong positive ROEs, suggesting the presence of a bound water (Wat^{304}). The amide of Arg^{149}, however, is attenuated by only 11-fold in control spectra, thus creating some ambiguity. In the crystal structure this water molecule is hydrogen bonded to the NH of Arg^{149} and the $O^{\delta 2}$ of Asp^{183}. These water molecules may increase the stability of the 15-residue loop that contains two of the structural zinc ligands, His^{151} and Asp^{153}. A third tightly bound water is suggested by a positive ROE to the NH of Ile^{101}, and corresponds to Wat^{302} in the crystal structure, which is hydrogen bonded only to the carbonyl of Leu^{135}. This amide, however, is attenuated by 11-fold in the control experiment, indicating some ambiguity.

The region Tyr^{223}–Arg^{231} forms the base and opening of the S1' subsite. The bottomless character of this subsite indicates that it is accessible to water. The NH protons of Ser^{225}, Thr^{227}, Asp^{228} and Leu^{229} all show strong negative ROEs to the water resonance (Fig. 10A), indicating that these amide protons are accessible to water, but are in chemical exchange with water. This observation is in agreement with the mobility of this loop and the fast amide exchange rates (Table 4). No ROEs/NOEs were observed to other amide protons in this region. Several methyl groups belonging to Leu^{222}, Leu^{226} and Leu^{227} are in or near the S1' subsite and are accessible to water (> 20 $Å^2$). Other methyl groups of residues Leu^{197}, Leu^{218} and Val^{198}, which are also in the S1' subsite, are relatively inaccessible to solvent. In Fig. 10B a peak is observed from water to the resonance of $C^{\delta 1}H_3$ of Leu^{226}, which is degenerate with the $C^{\delta 2}H_3$ of Leu^{229}. A strong NOE was also observed to these methyls, which was attenuated at least 20-fold in control spectra, indicating that one or both methyl groups are sites of methyl hydration (Clore et al., 1994).

Strong positive ROEs were observed to the amides of Lys^{94}, Tyr^{136} and Phe^{210} (Fig. 10A) and the methyls of Ala^{147}, Leu^{135}, Leu^{209} and Ala^{213} (Fig. 10B). The NH of Ala^{213} is near the carboxylate of Asp^{237} and the $C^{\delta 2}H_3$ of Leu^{135} is near the $H^{\gamma 1}$ of Thr^{98}. This latter group resonates at 5.24 ppm and is therefore not affected by the selective inversion pulse. The other groups are distant from exchangeable protons; however, all these peaks were attenuated by fourfold or less in the control experiments, suggesting that the ROEs are not to water. The ROEs assigned to Leu^{209} and Phe^{210} may be to the NH of His^{211}, which has not been observed under the solution conditions used here, and may resonate at the water frequency. The methyls of Leu^{135} and the NH of Tyr^{136} are near each other, suggesting that the ROEs are probably attributable to the same phenomenon. The reasons for persistence of these peaks in the control experiments are not clear, although incomplete ^{13}C labeling cannot be discounted.

Cleavage mechanism

Comparison of the structures of several MMPs complexed with inhibitors has suggested a common mechanism that involves nucleophilic attack of the scissile bond of a peptide by activated water, similar to that of thermolysin (Mathews, 1988). These mechanisms have been described in detail for fibroblast collagenase (Lovejoy et al., 1994; Spurlino et al., 1994) and for stromelysin-1 (Gooley et al., 1994; Becker et al., 1995). The essential residues involved in substrate cleavage by stromelysin-1 are included in Fig. 8A. The carbonyl and amide of the scissile bond form noncovalent bonds with the zinc and the carbonyl of Ala^{165} (or its equivalent in collagenase), respectively. Nucleophilic attack of the peptide is initiated by polarization of water by Glu^{202} and the catalytic zinc. The intermediates are stabilized by the carbonyl of Ala^{165}, the carboxylate of Glu^{202} and the zinc. In thermolysin additional residues, Tyr^{157} and His^{231}, play important roles in stabilizing the intermediates; however, equivalent residues to this tyrosine and histidine in stromelysin-1 or collagenase have not been observed. The side-chain carbonyl of Asn^{112} of thermolysin and of Asn^{180} of fibroblast collagenase further stabilizes the NH_2^+ intermediate; however, in stromelysin-1 the equivalent residue, Asn^{162}, does not play a similar role. The difference between fibroblast collagenase and stromelysin-1 is the replacement of Asn^{180} with Val^{163} in the latter protein, positioning Asn^{162} distant from the scissile bond of the substrate (Fig. 8A). This asparagine is not conserved and is absent in the sequences of neutrophil collagenase and the gelatinases, and thus its role in the mechanism of fibroblast collagenase is perhaps secondary.

The solution structure is completely consistent with the above interpretations, except that the significance of Glu^{202} is not readily apparent because χ^2 for this residue is not ordered (not shown). The disorder of Glu^{202} is reflected by a lack of unambiguous intraresidue and the presence of only a few interresidue NOEs for the side-chain protons. The poor intraresidue NOE data may be a result of spin diffusion at 50 ms mixing times; however, shorter mixing times (25 ms) failed to yield useable data. It is notable that the side-chain atoms of Glu^{202} were assigned in 3D NOESY and HNHb spectra and were not observed in 3D HCCH COSY and TOCSY spectra, suggesting that this side chain may be undergoing some dynamic process. Another possibility is that the pH of the NMR experiments (5.5) is near the pK_a of Glu^{202}; however, the carboxylate is expected to be electron donating in a hydrogen bond with the P1' amine of the inhibitor and thus its pK_a should be less than 4.

Conclusions

The refined NMR solution and X-ray crystal structures of the catalytic domain of stromelysin-1 complexed with

the same inhibitor have been compared. The fold and structural details, including the unusual features of the distortion of the consensus region HEIGH, the ϕ,ψ angles of Ile^{89}, Arg^{149} and Asn^{162} and the bottomless S1' subsite are observed in both structures. While the general similarity is satisfying, there are a number of significant differences, usually in poorly defined regions. Two of these regions may influence alternate routes to improve the potency of the inhibitor: the conformation of the region Tyr^{223}–Arg^{231}, and the presence or absence of the hydrogen bond between the carbonyl of P3' and the NH of Tyr^{223}. These poorly defined regions are generally a result of a lack of NOE data. In the region Tyr^{223}–Arg^{231}, where flexibility may contribute to the absence of short- and long-range NOEs, the family of solution structures does not include the crystal structure, suggesting that differences may lie in the treatment of experimental data. The flexibility of this region is currently being investigated in different inhibited forms of sfSTR.

Acknowledgements

We like to thank Dr. James P. Springer for his support throughout this study and Dr. Bruce A. Johnson for both his interest and continued development of his superlative program NMRView.

References

Archer, S.J., Ikura, M., Torchia, D.A. and Bax, A. (1991) *J. Magn. Reson.*, **95**, 636–641.

Baumann, U. (1994) *J. Mol. Biol.*, **242**, 244–251.

Becker, J.W., Marcy, A.I., Rokosz, L.L., Axel, M.G., Burbaum, J.J., Fitzgerald, P.M.D., Cameron, P.M., Esser, C.K., Hagmann, W.K., Hermes, J.D. and Springer, J.P. (1995) *Protein Sci.*, **4**, 1966–1976.

Bode, W., Gomis-Rüth, F.X., Huber, R., Zwilling, R. and Stöcker, W. (1992) *Nature*, **358**, 164–167.

Bode, W., Gomis-Rüth, F.X. and Stöcker, W. (1993) *FEBS Lett.*, **331**, 134–140.

Bode, W., Reinemer, P., Huber, R., Kleine, T., Schnierer, S. and Tschesche, H. (1994) *EMBO J.*, **13**, 1263–1269.

Borkatoti, N., Winkler, F.K., Williams, D.H., D'Arcy, A., Broadhurst, M.J., Brown, P.A., Johnson, W.H. and Murray, E.J. (1994) *Nature Struct. Biol.*, **1**, 106–110.

Brown, S.I., Weller, C.A. and Wasserman, H.E. (1969) *Arch. Ophthalmol.*, **81**, 370–373.

Brünger, A. (1992) *X-PLOR Manual, v. 3.1, A system for X-ray Crystallography and NMR*, Yale University Press, New Haven, CT.

Burgering, M., Boelens, R. and Kaptein, R. (1993) *J. Biomol. NMR*, **3**, 709–714.

Chapman, K.T., Kopka, I.E., Durette, P.L., Esser, C.K., Lanza, T.J., Izquierdo-Martin, M., Niedzwiecki, L., Chang, B., Harrison, R.K., Kuo, D.W., Lin, T.-Y., Stein, R.L. and Hagmann, W.K. (1993) *J. Med. Chem.*, **36**, 4293–4301.

Clore, G.M., Bax, A., Omichinski, J.G. and Gronenborn, A.M. (1994) *Structure*, **2**, 89–94.

Dean, D.D., Martel-Pelletier, J., Pelletier, J.-P., Howell, D.S. and Woessner, J.F. (1989) *J. Clin. Invest.*, **84**, 678–685.

Delaglio, F., Grzesiek, S., Vuister, G.W., Zhu, G., Pfeifer, J. and Bax, A. (1995) *J. Biomol. NMR*, **6**, 277–293.

Dumermuth, E., Sterchi, E.E., Jiang, W., Wolz, R.L., Bond, J.S., Flannery, A.V. and Beynon, R.J. (1991) *J. Biol. Chem.*, **266**, 21381–21385.

Engh, R.A. and Huber, R. (1991) *Acta Crystallogr.*, **A47**, 392–400.

Fox, J.W., Campbell, R., Beggerly, L. and Bjarnason, J.B. (1986) *Eur. J. Biochem.*, **156**, 65–72.

Gomis-Rüth, F.X., Kress, L.F. and Bode, W. (1993a) *EMBO J.*, **12**, 4151–4157.

Gomis-Rüth, F.X., Stöcker, W., Huber, R., Zwilling, R. and Bode, W. (1993b) *J. Mol. Biol.*, **229**, 945–968.

Gooley, P.R., Johnson, B.A., Marcy, A.I., Cuca, G.C., Salowe, S.P., Hagmann, W.K., Esser, C.K. and Springer, J.P. (1993) *Biochemistry*, **32**, 13098–13108.

Gooley, P.R., O'Connell, J.F., Marcy, A.I., Cuca, G.C., Salowe, S.P., Bush, B.L., Hermes, J.D., Esser, C.K., Hagmann, W.K., Springer, J.P. and Johnson, B.A. (1994) *Nature Struct. Biol.*, **1**, 111–118.

Grams, F., Reinemer, P., Powers, J.C., Kleine, T., Pieper, M., Tschesche, H., Huber, R. and Bode, W. (1995) *Eur. J. Biochem.*, **228**, 830–841.

Gravallese, E.M., Darling, J.M., Ladd, A.L. and Katz, J.N. (1991) *Arthritis Rheum.*, **34**, 1076–1084.

Gregoret, L.M., Rader, S.D., Fletterick, R.J. and Cohen, F.E. (1991) *Proteins*, **9**, 99–107.

Grzesiek, S. and Bax, A. (1993a) *J. Am. Chem. Soc.*, **115**, 12593–12594.

Grzesiek, S. and Bax, A. (1993b) *J. Biomol. NMR*, **3**, 627–638.

Güntert, P., Braun, W., Billeter, M. and Wüthrich, K. (1989) *J. Am. Chem. Soc.*, **111**, 3997–4004.

Güntert, P., Braun, W. and Wüthrich, K. (1991) *J. Mol. Biol.*, **217**, 517–530.

Güntert, P. and Wüthrich, K. (1991) *J. Biomol. NMR*, **1**, 447–456.

Häse, C.C. and Finkelstein, R.A. (1994) *Microbiol. Rev.*, **57**, 823–837.

Hasty, K.A., Reife, R.A., Kang, A.H. and Stuart, J.M. (1990) *Arthritis Rheum.*, **33**, 388–397.

Ho, T.F., Qoronfleh, M.W., Wahl, R.C., Pulvino, T.A., Vavra, K.J., Falvo, J., Banks, T.M., Brake, P.G. and Ciccarelli, R.B. (1994) *Gene*, **146**, 297–301.

Holmes, M.A. and Mathews, B.W. (1982) *J. Mol. Biol.*, **160**, 623–639.

Ikura, M., Kay, L.E., Tschudin, R. and Bax, A. (1990) *J. Magn. Reson.*, **86**, 204–209.

Ito, A. and Nagase, H. (1988) *Arch. Biochem. Biophys.*, **267**, 211–216.

Izquierdo-Martin, M., Chapman, K.T., Hagmann, W.K. and Stein, R. (1994) *Biochemistry*, **33**, 1356–1365.

Johnson, B.A. and Blevins, R.A. (1994) *J. Biomol. NMR*, **4**, 603–614.

Kabsch, W. and Sander, C. (1983) *Biopolymers*, **22**, 2577–2637.

Leszczynski, J.F. and Rose, G.D. (1986) *Science*, **234**, 849–855.

Lovejoy, B., Cleasby, A., Hassell, A.M., Longley, K., Luther, M.A., Weigl, D., McGeehan, G., McElroy, A.B., Drewry, D., Lambert, M.H. and Jordan, S.R. (1994) *Science*, **263**, 375–377.

Marcy, A.I., Eiberger, L.L., Harrison, R., Chan, H.K., Hutchinson, N.I., Hagmann, W.K., Cameron, P.M., Boulton, D.A. and Hermes, J.D. (1991) *Biochemistry*, **30**, 6476–6483.

Mathews, B.W. (1988) *Acc. Chem. Res.*, **21**, 333–340.

Matrisian, L.M., Bowden, G.T., Krieg, P., Furstenberger, G., Briand, J.P., Leroy, P. and Breathnach, R. (1986) *Proc. Natl. Acad. Sci. USA*, **83**, 9413–9417.

McCachren, S.S., Haynes, B.F. and Niedel, J.E. (1990) *J. Clin. Immunol.*, **10**, 19–27.

McCoy, M.A. and Mueller, L. (1992) *J. Magn. Reson.*, **98**, 674–679.

Morris, A.L., MacArthur, M.W., Hutchinson, E.G. and Thornton, J.M. (1992) *Proteins*, **12**, 345–364.

Murphy, G., Cockett, M.I., Stephens, P.E., Smith, B.J. and Docherty, A.J.P. (1987) *Biochem. J.*, **248**, 265–268.

Murphy, G.J.P., Murphy, G. and Reynolds, J.J. (1991) *FEBS Lett.*, **289**, 4–7.

Neri, D., Szyperski, T., Otting, G., Senn, H. and Wüthrich, K. (1989) *Biochemistry*, **28**, 7510–7516.

Okada, Y., Shinmei, M., Tanaka, O., Naka, K., Kimura, A., Nakanishi, I., Bayliss, M.T., Iwata, K. and Nagase, H. (1992) *Lab. Invest.*, **66**, 680–690.

Otting, G., Liepinsh, E. and Wüthrich, K. (1991) *Science*, **254**, 974–980.

Overall, C.M., Wiebkin, O.W. and Thonard, J.C. (1987) *J. Periodontal Res.*, **22**, 81–88.

Powers, R., Gronenborn, A.M., Clore, G.M. and Bax, A. (1991) *J. Magn. Reson.*, **94**, 209–213.

Richardson, J.S. (1977) *Nature*, **268**, 495–500.

Salowe, S.P., Marcy, A.I., Cuca, G.C., Smith, C.K., Kopka, I.E., Hagmann, W.K. and Hermes, J.D. (1992) *Biochemistry*, **31**, 4535–4540.

Schaumann, T., Braun, W. and Wüthrich, K. (1990) *Biopolymers*, **29**, 679–694.

Spera, S., Ikura, M. and Bax, A. (1991) *J. Biomol. NMR*, **1**, 155–165.

Spitzfaden, C., Braub, W., Wider, G., Widmer, H. and Wüthrich, K. (1994) *J. Biomol. NMR*, **4**, 463–482.

Spurlino, J.C., Smallwood, A.M., Carlton, D.D., Banks, T.M., Vavra, K.J., Johnson, J.S., Cook, E.R., Falvo, J., Wahl, R.C., Pulvino, T.A., Wendoloski, J.J. and Smith, D.L. (1994) *Proteins*, **19**, 98–109.

Stams, T., Spurlino, J.C., Smith, D.L., Wahl, R.C., Ho, T.F., Qoronfleh, M.W., Banks, T.M. and Rubin, B. (1994) *Nature Struct. Biol.*, **1**, 119–123.

Stöcker, W., Grams, F., Baumann, U., Reinemer, P., Gomis-Rüth, F.X., McKay, D.B. and Bode, W. (1995) *Protein Sci.*, **4**, 823–840.

Suri, A.K. and Levy, R.M. (1993) *J. Magn. Reson.*, **101**, 320–324.

Vuister, G.W., Delaglio, F. and Bax, A. (1992) *J. Am. Chem. Soc.*, **114**, 9674–9675.

Vuister, G.W. and Bax, A. (1993) *J. Am. Chem. Soc.*, **115**, 7772–7777.

Wagner, G., Hyberts, S. and Peng, J.W. (1993) In *Topics in Molecular and Structural Biology: NMR of Proteins: Study of Protein Dynamics by NMR* (Eds, Clore, G.M. and Gronenborn, A.M.), CRC Press, Boca Raton, FL, pp. 220–257.

Welgus, H.G. (1991) In *Progress in Inflammation: Research and Therapy* (Eds, Ackermann, N., Bonney, R.J. and Welton, A.F.), Birkhauser Verlag, Boston, MA, pp. 61–67.

Widmer, H., Widmer, A. and Braun, W. (1993) *J. Biomol. NMR*, **3**, 307–324.

Woessner, J.D. (1991) *FASEB J.*, **5**, 2145–2154.

Wu, J.-J., Lark, M.W., Chun, L.E. and Eyre, D.R. (1991) *J. Biol. Chem.*, **266**, 5625–5628.

Xia, T.H. (1992) Ph.D. Thesis, ETH, Zürich.

Zhang, D.C., Botos, I., Gomis-Rüth, F.X., Doll, R., Blood, C., Njoroge, F.G., Fox, J.W., Bode, W. and Meyer, E.F. (1994) *Proc. Natl. Acad. Sci. USA*, **91**, 8447–8451.

Zuiderweg, E.R.P. and Fesik, S. (1989) *Biochemistry*, **28**, 2387–2391.